Disclaimer: This is not the final version of the article. Changes may occur when the manuscript is published in its final format.

Computational Identification of Epitopes from Sindbis Virus E1, E2, and Capsid Proteins for Multi-Epitope Vaccine Design

Emmanuel Oladiran Amos[1*], Olufemi Samuel Araoyinbo[2], Suleiman Oluwaseun Alakanse[1,3], Enoch Olanrewaju Akinleye[1], Oluwaseun Olaniyi Olalere[4], Joy Faiza Sule[3], Olatunji Matthew Kolawole[5,6]

[1]Department of Biochemistry, Faculty of Life Sciences, University of Ilorin, Ilorin, Nigeria.

[2]Department of Chemistry and Biochemistry, Florida State University, Tallahassee, United States.

[3]Department of Biotechnology, Federal University Lokoja, Lokoja, Nigeria.

[4]Research Institute of the McGill University Health Centre, Montreal, Quebec, Canada.

[5]Department of Microbiology, Faculty of Life Sciences, University of Ilorin, Ilorin, Nigeria.

[6]Department of Public Health, Warwick Medical School, University of Warwick, United Kingdom.

*Correspondence: emmanuelamos321@gmail.com , +2348167273003

Co-correspondence: omk@unilorin.edu.ng, +2348060088495

Abstract

Sindbis virus (SINV) is taxonomically classified under the *Alphavirus* genus and is transmitted by mosquito vectors. It causes a febrile illness that is characterized by rash and arthralgia and currently lacks a licensed vaccine. To address this unmet need, predictive immune modelling techniques were utilize to construct a vaccine formulation targeting the conserved and immunogenic regions of the viral E1, E2, and capsid proteins. Antigenicity assessment guided the selection of eighteen epitopes, comprising six cytotoxic T lymphocyte (CTL), six helper T lymphocyte (HTL) and six B-cell epitopes. These epitopes were assembled using peptide linkers and supplemented with the 50S ribosomal protein L7/L12 as an adjuvant. Three-dimensional structural validation using ProSA Z-score, QMEAN4, Ramachandran plot and ERRAT analyses indicated acceptable structural quality. Subsequent protein–protein docking predicted structural interactions between the vaccine construct and TLR2/4/7/8, and MHC class I and II molecules. Normal mode analysis further provided insights into the predicted flexibility and collective motions of the modelled vaccine–receptor complexes. *In silico* immune simulation predicted changes in antibody titres, cytokine profiles and both innate and adaptive immune-cell populations over 35 days following a single simulated vaccination. Furthermore, successful *In silico* cloning of the multi-epitope vaccine (MEV) into the pYES2 vector further suggested its potential expression feasibility. Overall, these computational findings suggest that the proposed construct may elicit immune responses, retain an appropriate predicted structural conformation and be amenable to expression. These findings support its prioritization as a candidate for further experimental investigations to establish its immunogenicity, safety and protective efficacy against relevant SINV strains.

Keywords: Sindbis virus (SINV); capsid protein; E1 and E2 glycoproteins; multi-epitope vaccine; epitope prediction; protein-protein docking.

1. Introduction

Sindbis virus (SINV) is an enveloped arbovirus possessing a positive-sense single-stranded Ribonucleic acid (RNA) genome. According to [1], it is taxonomically classified under the Alphavirus genus of the Togaviridae family. The viral genome is approximately 11.7 kilobyte in length and is organized into two open reading frames that encode four non-structural proteins (nsP1–nsP4) and five structural proteins, including the capsid (C) and envelope-associated proteins (E1, E2, E3 and 6K/TF) [2,3]. Phylogenetic sequence characterization of the partial E2 gene has identified six genetically distinct genotypes of SINV [4,5], of which genotype I has been most frequently implicated in human disease outbreaks. Surveillance data indicates SINV's first recognition as a human pathogen in 1961 following its isolation from a patient that presented with high fever in Uganda [6].

The viral infection resulting from SINV is referred to by various names across the northern Europe —in Finland it is Pogosta and Sweden Ockelbo disease. The disease affects individuals across all age groups and shows no marked sex-related differences in incidence [7]. Its clinical presentation includes symptoms such as fever, headaches, meningitis, rash, and joint pain, which may persist for prolonged periods [6]. Following the bite of an infected mosquito, the transmitted virus interacts with host-cell receptors to initiate entry, migrate to the lymph nodes and replicates before disseminating to the joints and other internal organs [8].

Despite episodic outbreaks, SINV infection still remains potentially underdiagnosed, particularly in non-endemic regions where few cases are reported [6,9]. Moreover, the underlying factors driving and sustaining the outbreaks in regions with a high incidence of SINV remain poorly understood [2,9]. Recent detections of SINV in Africa and Europe highlight the importance of continued surveillance [5,10,11]. Although climate change, environmental shifts, and altered

vector ecology may influence arbovirus distribution, their specific contributions to the geographic distribution of SINV require further investigation [12,13]. In addition, the full burden of SINV infection particularly in terms of its febrile and neurological manifestations remains inadequately characterized [6]. Current prevention and control measures in endemic regions are largely limited to public awareness campaigns promoting mosquito-bite avoidance. Crucially, no specific antiviral therapy or licensed vaccine is currently available for the treatment or prevention of SINV infection [8,14]. To date, the management of symptoms remains largely supportive, focusing on pain relief without directly addressing the underlying viral infection [8].

A successful vaccine design will require the identification of immunologically relevant Sindbis virus antigens that may induce protective immune responses [15]. Research has elucidated the multifaceted roles of capsid, E1, and E2 structural proteins in viral entry, modulation of host immune responses and the packaging and assembly of the viral genome [14,16]. The capsid protein contributes to viral assembly and has been implicated in the evasion of innate immune responses through IRAK1 inhibition [17]. During viral entry, membrane fusion is mediated by the E1 envelope protein, whereas E2 plays a central role in host-cell attachment and constitutes a major target of the humoral immune response [4]. These features collectively underpin the selection of capsid, E1, and E2 as candidate antigen sources in this study. E3 was excluded because it is cleaved during envelope-protein processing and has limited association with the mature virion, whereas nsP1–nsP4 were excluded because this study focuses on structural proteins involved in virion architecture, entry, and assembly rather than non-structural proteins involved primarily in viral replication.

Computational approaches have increasingly contributed to antigen discovery and vaccine design by integrating sequence-based epitope prediction with structural and molecular-interaction

analyses. Recent computational investigations have integrated structural analysis, docking and complementary theoretical approaches to characterize viral or biologically relevant molecular targets, including studies involving viral capsid-associated systems and protein–ligand interactions [18–21]. These developments illustrate the increasing utility of computational modelling for prioritizing candidate molecular targets before experimental investigation.

Within arbovirology, multi-epitope vaccine strategies have been explored for several mosquito-borne alphaviruses, including O'nyong-nyong virus, Ross River virus, Mayaro virus and Chikungunya virus [22–24]. However, computational vaccine development for Sindbis virus remains comparatively limited. A recent study by [14] provided an important proof of concept for multi-epitope vaccine development against SINV. Nevertheless, systematic prioritization of candidate epitopes according to their immunological properties and conservation across genetically diverse SINV strains remains insufficiently explored. This gap is particularly relevant because sequence variation among geographically and phylogenetically distinct SINV strains may influence the potential breadth of epitope coverage achievable by an epitope-based vaccine. The novelty of the present study lies in integrating immunological epitope prioritization with cross-strain conservation analysis before vaccine construct assembly, enabling the evaluation of candidate epitopes across a genetically diverse SINV sequence panel. The study further integrates structural modelling, receptor-interaction analysis, normal mode analysis, immune simulation, and in silico expression assessment to provide an integrated computational evaluation of the resulting multi-epitope vaccine candidate against SINV.

2. Materials and Methods

2.1. Retrieval of the Target Sequences

Sindbis virus proteomic sequence utilized for this study were downloaded from the Universal Protein Resource database (UniProt). The reference SINV proteome (UniProt identifier: UP000006710) was selected, as it represents the curated and consensus protein sequences for the species. To ensure that the selected proteins adequately represent global SINV diversity, additional E1, E2, and capsid sequences were obtained from ten genetically diverse SINV strains belonging to genotypes G1, G2, G4, G6 and SINV-like lineages. These strains span multiple geographic regions, including Africa, Europe, Asia, and Australia (GenBank accession numbers: NC_001547.1, AF429428.1, AF103728.1, OK491658.1, MH212167.1, M69205, AF103734, U38305, PP889333, J02363.1). This panel was selected to capture broad phylogenetic and geographic variation reported for SINV.

2.2. CTL Epitope Prediction and Evaluation

The identification of CTL–responsive peptides is a critical prerequisite for rational multi-epitope vaccine construction. To this end, putative MHC I binding epitopes were computationally identified using the class I T-cell epitope prediction framework hosted within the Immune Epitope Database resource [25]. The FASTA sequence of the Sindbis virus were submitted to the prediction tool. Epitope prediction was performed using a neural network–based binding affinity model (NetMHCpan, EL mode, version 4.1; 2023 release), with candidate peptides filtered using a stringent percentile rank cutoff of ≤1%. The MHC source was designated as human, and the peptide length setting was to identify candidate peptides containing potential MHC class I-binding regions. The NetMHCpan EL prediction model estimates peptide presentation potential based on

eluted ligand data and provides predicted binding core regions within the submitted peptide sequences. Accordingly, the full peptide sequences reported in the prediction output were used for subsequent candidate evaluation, while the corresponding predicted core regions were used to characterize potential MHC class I-binding regions. The twenty-seven (27) frequently occurring class I human leucocyte antigen alleles for this prediction includes: HLA-A*01:01, HLA-A*02:01, HLA-A*02:03, HLA-A*02:06, HLA-A*03:01, HLA-A*11:01, HLA-A*23:01, HLA-A*24:02, HLA-A*26:01, HLA-A*30:01, HLA-A*30:02, HLA-A*31:01, HLA-A*32:01, HLA-A*33:01, HLA-A*68:01, HLA-A*68:02, HLA-B*07:02, HLA-B*08:01, HLA-B*15:01, HLA-B*35:01, HLA-B*40:01, HLA-B*44:02 HLA-B*44:03 HLA-B*51:01, HLA-B*53:01, HLA-B*57:01, HLA-B*58:01). The ≤1% percentile rank threshold was applied as a stringent initial screening criterion for candidate CTL epitopes. Upon further filtering of the predicted peptides, only those with antigenicity scores >0.5 and immunogenicity scores >0.01, and those predicted to be non-allergenic and non-toxic, were retained.

2.3. HTL Epitope Prediction and Evaluation

This step supports the identification of peptides with high MHC II binding potential across range of HLA alleles to guide the development of vaccine that can both target immunogenicity and also maximize broad population applicability. Candidate MHC class II molecules were identified using the class II prediction framework available through the Immune Epitope Database platform (https://nextgen-tools.iedb.org/). Sindbis virus protein sequences, provided in FASTA format, were analyzed using the 2023 release of the IEDB-recommended NetMHCIIpan version 4.1 pan-allelic binding prediction model. The selected prediction parameters were a percentile rank threshold of top 10%, peptide length of 15 and reference panel comprising 27 HLA class II alleles [26]. The ≤10% percentile rank threshold was applied during initial screening to capture a broader

range of candidate MHC class II binders for subsequent evaluation. The full peptide sequences reported in the prediction output were used for subsequent candidate evaluation, while the corresponding predicted core regions provided information on potential MHC class II-binding regions. To further assess predicted binding strength, selected epitopes were re-evaluated using the additional binding-strength assessment described in this study. The resulting epitopes were further examined for antigenic potential and their predicted allergenic and toxic characteristics, and candidates were retained according to the applied immunological selection criteria.

2.4. B-cell Epitope Prediction and Evaluation

Recognition of antigens regions by B-cell receptors is essential to eliciting effective humoral immune responses. Linear B-cell epitope regions within the protein sequences were identified using a motif-based scanning approach implemented in the CLBTope scan module (https://webs.iiitd.edu.in/raghava/clbtope/#protein). Hybrid prediction method, a fusion of Dipeptide Composition (DPC) and Blast according to [27] was applied. The prediction parameters utilized were 0.53 threshold value and 16 peptide length. The resulting epitopes were further examined to evaluate their ability antigenic potential, as well as their, allergenic and toxic characteristics.

2.5. Antigenicity, Immunogenicity, Allergenicity and Toxicity Assessment

All shortlisted epitopes incorporated into the multi-epitope vaccine construct were subjected to a multi-parameter screening process to ensure their suitability for inducing immune responses while minimizing allergenic and toxic risks. Antigenic potential was evaluated using an alignment-independent prediction model based on physicochemical properties, implemented via the VaxiJen 2.0 platform (https://www.ddg-pharmfac.net/vaxijen/VaxiJen/VaxiJen.html), with a cutoff score

of 0.5 applied to distinguish antigenic from non-antigenic sequences [28]. Using a threshold value set at 0.01, the immunogenic and allergenic properties of the predicted peptides were subsequently assessed using a machine learning–based classification framework on the version 2.1 AllerTOP tool (https://www.ddg-pharmfac.net/allertop_test/). According to [29], this online server employs auto-cross covariance transformation to encode protein sequences into uniform numerical descriptors for predictive analysis. In parallel, peptide–MHC class I complex immunogenicity was estimated using a position-specific amino acid–based model available through the IEDB immunogenicity prediction resource (http://tools.iedb.org/immunogenicity/). Potential peptide toxicity was evaluated using a ToxinPred quantitative toxicity prediction framework designed for peptide sequence analysis (https://webs.iiitd.edu.in/raghava/toxinpred/design.php).

2.6. Epitope Conservancy Analysis

Conservancy analysis calculates epitope distribution and the degree of sequence similarity across different strains. To assess the degree of sequence conservation among the prioritized CTL, HTL, and B-cell epitopes, conservancy analysis was performed using the epitope conservancy evaluation framework provided by the Immune Epitope Database (https://tools.iedb.org/conservancy/). . Ten SINV structural-protein sequence datasets archived in GenBank were deliberately selected to capture genetic and geographic diversity across the analysed strains and lineages. The selected GenBank accession numbers were NC_001547.1, AF429428.1, AF103728.1, OK491658.1, MH212167.1, M69205, AF103734, U38305, PP889333, and J02363.1. For this analysis, the 18 selected epitopes used to assemble the vaccine were uploaded and the corresponding sequences from the 10 divergent SINV lineages concurrently supplied in plain FASTA format. An identity threshold of $\geq$ 80% was applied to ensure robust selection of evolutionarily conserved epitopes across analyzed sequences.

2.7. Multi-epitope Vaccine Mapping

In accordance with the design framework established by [30], the multi-epitope vaccine was organized from the N-terminal, beginning with an adjuvant then followed by six CTL, HTL and B-cell epitopes each. These epitopes were linked together through short EAAAK, AAY, GPGPG and KK peptide linkers according to the order described by [30]. The sequence (UniRef100_UPI0005A61EDB) was incorporated into the vaccine construct as an immunostimulatory carrier adjuvant based on its documented capacity to enhance antigen immunogenicity and support innate immune activation in vaccine designs [30,31]. L7/L12 has been previously employed in subunit vaccine constructs as a carrier adjuvant to promote the presentation of antigen without implying strict receptor-specific ligand recognition. Cross-reactivity screening analysis against the Homo sapiens proteome was conducted using human RefSeq database (taxid: 9606) with standard gap penalties, BLOSUM62 as the scoring matrix, and a threshold E-value of 1×10^{-5}.

2.8. Physicochemical Properties and Secondary Structure Prediction

The protein sequence of the vaccine was uploaded and processed through different prediction tools and analysis conducted with default configurations across all the predictions. Physicochemical parameters and secondary structure analysis was predicted by the ProtParam tool and PSIPRED tool. The SoDoPE tool predicted the solubility of the vaccine while the Protein sol tool was utilized to validate the prediction. The PSIPRED secondary structure prediction tool to analyze Position-Specific Iterative Basic Local Alignment Search Tool (PSI-BLAST) output for accurate identification of protein helices, strands, and coils [32]. The SOPMA online tool further analyze the amino acid sequence based for it secondary structure.

2.9. Tertiary Structure Modeling

The three-dimensional conformational of the vaccine was modelled on the I-TASSER online web tool (https://zhanggroup.org/I-TASSER/). According to [33], this modeling tool builds possible shapes from small known templates, compares them with structures from the Research Collaborator for Structural Bioinformatics Protein repository and then select 10 best matching shapes. Following structural assembly, I-TASSER generates multiple conformations, which are clustered using the SPICKER program based on pairwise structure similarity [34]. Five representative models from the largest groups are selected then assign a confidence value. A higher value is more reliable and signifies better confidence. Subsequently, the length of the protein sequence and C-score were used for the estimation of Root-Mean-Square Deviation (RMSD) and Template Modeling score (TM-score) parameters.

2.10. Tertiary Structure Refinement and Validation

Further refinement of the structure generated from I-TASSER server was carried out in order to achieve structural accuracy that is comparable to experimental result. The predicted vaccine structure file was uploaded to the GalaxyWeb tool (https://galaxy.seoklab.org/) for the refinement analysis. The refinement process involves structural perturbation, relaxation, and side-chain repacking to improve local geometry and side-chain conformations. Model 1 was selected for subsequent structural validation and downstream analyses based on the returned model order, its lowest MolProbity score, and the fewest poor rotamers among the five models generated [35]. Following the refinement process, the selected refined model was subjected to structural validation steps. Two independent protein analysis tools (https://saves.mbi.ucla.edu/) and (https://prosa.services.came.sbg.ac.at/prosa.php) were implemented to study the predicted 3D

structure and three different plots were generated to measures structural integrity and stereo-chemical quality.

2.11. Discontinuous B-cell Epitope Prediction

IEBD Ellipro prediction platform (http://tools.iedb.org/ellipro/) predicted both the linear and discontinuous epitopes corresponding to the conformational structure of the engineered vaccine construct. Vaccine structure in PDB format was uploaded with default parameters of 0.5 minimum score and 6 Å maximum distance. According to description by [36], the prediction method is such that ElliPro tool approximates protein structure using a series if ellipsoids, where an ellipsoid with 0.9 protrusion index (PI) would include 90% approximate of the protein residues. Averaged protrusion index (PI) scores was utilized to rank each predicted epitopes accordingly.

2.12. Disulfide Engineering of the Vaccine Structure

To enhance the structural stability of the designed multi-epitope vaccine, disulfide engineering was performed to identify residue pairs suitable for cysteine substitution and potential disulfide bond formation. The analysis was conducted using Disulfide by Design 2 tool (DbD) (http://cptweb.cpt.wayne.edu/DbD2/), which predicts candidate residue pairs based on geometric and energetic constraints. Residue pairs were evaluated according to established criteria, including $\chi 3$ dihedral angle ($+97° \pm 30°$ and $-87° \pm 30°$), bond energy, and spatial proximity formation [37]. Only pairs exhibiting favorable $\chi 3$ values within the permissible range and low bond energy were considered for mutation, as these parameters are indicative of stable and geometrically feasible disulfide bond formation [37]. In addition, residues such as glycine and proline were excluded due to their unfavorable conformational properties for disulfide bond formation.

2.13. Peptide Modeling and Molecular Docking

Molecular docking was applied to examine how the proposed vaccine construct may associate with key immune system components, specifically Toll-like receptors as well as major histocompatibility complex (MHC) molecules. PDB structures with attached ID: TLR7 (7CYN), TLR8 (3W3J), TLR2 (6NIG), TLR4 (2Z63), MHC I (1A1M) and MHC II (1AQD) were obtained from the RCSB repository. Protein–protein docking was performed using the ClusPro web server (https://cluspro.org/home.php) following its established protein–protein docking protocol [38]. The vaccine construct and each immune receptor were treated as protein docking partners, and the resulting docking models were evaluated based on the ClusPro clustering and scoring outputs [38]. The docking analyses involving TLR7 and TLR8 were intended to explore potential structural compatibility between the vaccine construct and these endosomal pattern-recognition receptors. Given the endosomal localization and physiological ligand-recognition context of TLR7 and TLR8, these docking predictions do not establish that the full vaccine construct can access or bind these receptors in vivo, nor do they demonstrate receptor activation. PEP-FOLD 3.0 tool was utilized to predict the 3D conformational structure of the E1 (KPGAFGDIQATSLTS) and E2 (ACKARRECLTPYAL) glycoprotein epitopes docked against the MHC I and MCH II molecules. PEP-FOLD 3.0 server builds 3D short-chain peptide structure from scratch without relying on structural templates [39]. The COCOMAPS 2.0 tool (https://aocdweb.com/BioTools/cocomaps2/) was utilized to conduct a detailed assessment of the binding interfaces and molecular interaction patterns between the vaccine and immune receptors [40,41]. According to the geometric criteria applied in the COCOMAPS analysis, interactions resulting from hydrophobic side-chain packing are classified as apolar van der Waals contacts, whereas CH–O/N contacts, salt bridges and hydrogen bonds are categorized as polar atomic interactions. Finally, the binding free energy (ΔG)

and dissociation constant (Kd) of the docked vaccine–receptor complexes were estimated using the PRODIGY web server (https://wenmr.science.uu.nl/prodigy/), to predicts binding affinity based on interfacial contacts and physicochemical properties of the complex.

2.14. Normal Mode Analysis using iMODS

The iMOD tool was utilized to investigate the collective atomic motions and conformational flexibility of the vaccine-receptor complexes at the molecular level. Normal Mode Analysis (NMA) was performed to examine the intrinsic motions and structural flexibility of the vaccine in complex with the TLR2, TLR4, TLR7, and TLR8 immune receptors. The docked complexes were submitted to the iMODS server in PDB format for analysis. NMA calculations were performed in torsional space with a maximum execution time of 10 min. Deformability plots, B-factor profiles, and eigenvalue parameters were generated to evaluate molecular flexibility, collective motions, and the energetic requirements associated with structural deformation [42,43].

2.15. Immune Simulation

The immune response to the vaccine constructs was modeled computationally using (http://kraken.iac.rm.cnr.it/C-IMMSIM) online platform. A single-dose vaccination model was simulated over 35-days period. To perform this simulation, upload of the sequence of the vaccine was done with all the parameters required for simulation set at default. The simulation generated graphical outputs representing immunoglobulins levels, cytokines and interleukins profiles, and population dynamics of various immune cell types following vaccine administration [44].

2.16. *In silico* Cloning

To evaluate the potential for efficient vaccine expression, this virtual cloning step was conducted to assess whether the optimized vaccine gene could be theoretically accommodated within a

standard bacterial expression vector. The amino acid sequence of the vaccine was converted into an optimized Deoxyribonucleic acid (DNA) sequence for efficient expression in the *Saccharomyces cerevisiae* host system. [45]'s method was implemented to assess expression efficiency parameters. The SnapGene software was implemented to simulate the cloning strategy for the potential experimental expression. The optimized DNA sequence was cloned into the pYES2 (+) expression vector precisely at the PvuII restriction site.

3. Results

3.1. Prediction of MHC class I and II binding epitopes

Initial epitope screening of Sindbis virus structural and capsid sequences resulted in the identification of 56,596 CTL epitopes and 7,591 HTL epitopes. Only 0.1% and 0.75% of the CTL and HTL epitopes were retained after applying stringent multi-step filtering criteria, including MHC binding percentile rank (CTL: NetMHCpan EL percentile ≤ 1%; HTL: NetMHCIIpan EL percentile ≤ 10%), antigenicity (VaxiJen ≥ 0.5), immunogenicity (CTL > 0.01), and exclusion of allergenic and toxic peptides. **Table 1** and **Table 2** shows the final selected CTL and HTL epitopes after all downstream analyses. A detailed summary of the selection workflow and associated numerical thresholds are provided in the Methods section and Supplementary Tables S1 and S2. Similarly, the corresponding optimal 8–11-mer binding core predicted by NetMHCpan EL for each selected CTL epitope can also be seen in Supplementary Table S1. Cytokine induction analysis of HTL epitopes using IFNepitope, IL2Pred, and IL4Pred tools revealed a mixed immunological profile, with selected epitopes showing IL-4–inducing potential, limited IFN-γ and no IL-2 induction at the individual peptide level (Supplementary Table S5).

Table 1: Final identified CTL Epitopes from E1, E2 and Capsid Protein and their corresponding properties. Residue positions refer to the corresponding individual protein sequences.

Protein	Epitope	Alleles	Start	End	Antigenic Score	Immunogenic Score	Allergenicity Score	Toxicity
E1 Glycoprotein	AGPISASFTPFDHK	HLA-A*11:01	163	176	1.3781	0.1350	Non-Allergen	Nontoxic
E1 Glycoprotein	ISASFTPFDHKVVI	HLA-B*51:01	166	179	1.1429	0.0102	Non-Allergen	Non-toxic
E2 Glycoprotein	ACKARRECLTPYAL	HLA-B*40:01	389	402	1.0317	0.1514	Non-Allergen	Non-toxic
E2 Glycoprotein	CTVYDRLKETTAGY	HLA-A*26:01	152	165	0.9961	0.0855	Non-Allergen	Non-toxic
Capsid Protein	DLPIGINITRFQTL	HLA-B*08:01	228	241	1.1058	0.5395	Non-Allergen	Non-toxic
Capsid Protein	VVFLHVTYVPAQEK	HLA-A*03:01	106	119	1.1069	0.15971	Non-Allergen	Non-toxic

Table 2: Final identified HTL Epitopes from E1, E2 and Capsid Protein and their corresponding properties. Residue positions refer to the corresponding individual protein sequences.

Protein	Epitope	Alleles	Start	End	Antigenic Score	Allergenic Score	Toxicity
E1 Glycoprotein	KPGAFGDIQATSLTS	HLA-DRB1*07:01	196	210	1.4608	Non-Allergen	Non-toxic
E1 Glycoprotein	PGAFGDIQATSLTSK	HLA-DRB1*07:01	197	211	1.3090	Non-Allergen	Non-toxic
E2 Glycoprotein	VPCFSPVKIEQVWDE	HLA-DRB1*07:01	23	37	1.0470	Non-Allergen	Non-toxic
E2 Glycoprotein	VYDRLKETTAGYITM	HLA-DRB1*07:01	154	168	0.7694	Non-Allergen	Non-toxic
Capsid Protein	DMEFAQLPVNMRSEA	HLA-DRB5*01:01	163	177	1.2167	Non-Allergen	Non-toxic
Capsid Protein	AYDMEFAQLPVNMRS	HLA-DRB5*01:01	161	175	1.1928	Non-Allergen	Non-toxic

3. 2. Prediction of Linear B-cell epitopes

The CLBTope server identified a total of 1,028 overlapping peptide epitopes from the structural and capsid proteins of Sindbis Virus following submission of their amino acid sequences. Detailed view of this peptides can be seen in Supplementary Table S3. Application of hybrid scoring criteria retained only 5.8% of the predicted epitopes, from which six highest-ranked epitopes demonstrating acceptable antigenicity, allergenicity and toxicity requirements were selected (**Table 3**).

Table 3: Final Identified B-cell Epitopes from Glycoprotein E1, E2 and Capsid Protein and their corresponding properties. Residue positions refer to the corresponding individual protein sequences.

Protein	Epitope Sequence	Antigenic Score	Allergenic Score	Toxicity
E1 Glycoprotein	ERAGYAPLNLEITVMS	1.5356	Non-Allergen	Non-toxic
E1 Glycoprotein	RAGYAPLNLEITVMSS	1.4830	Non-Allergen	Non-toxic
E2 Glycoprotein	SYCHHTVPCFSPVKIE	1.3419	Non-Allergen	Non-toxic
E2 Glycoprotein	CHHTVPCFSPVKIEQV	1.3025	Non-Allergen	Non-toxic
Capsid Protein	PRRRRQAAPMPARNGL	1.2411	Non-Allergen	Non-toxic
Capsid Protein	WRPRRRRQAAPMPARN	1.1132	Non-Allergen	Non-toxic

3.3. Construction of the Vaccine for Sindbis Virus

Figure 1 shows the framework and sequential arrangement of epitopes in the designed vaccine. The position of the immunostimulatory adjuvant (121 amino acids) is also showed. Overall, the primary structure comprised of 453 well-structured amino acids.

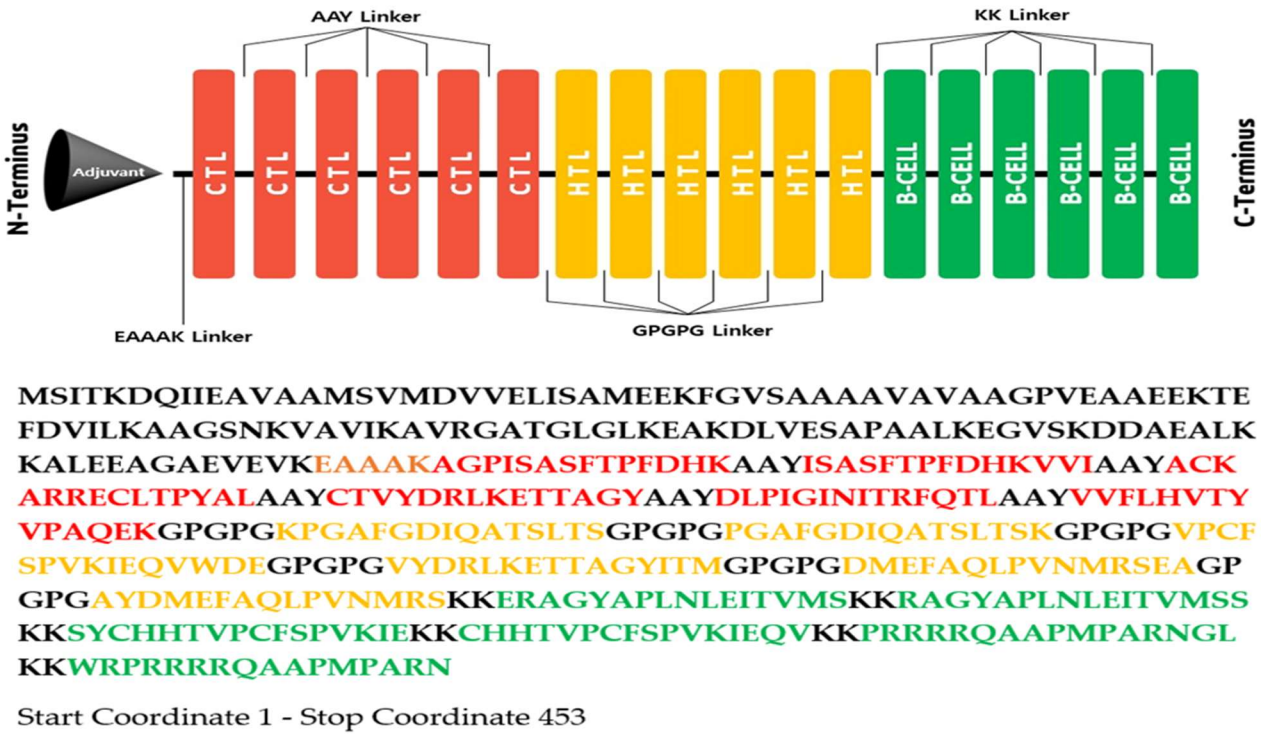


Figure 1: The sketch and proteomics sequence of the multi-epitope vaccine against Sindbis Virus.

3.4. Primary Structure Analysis of the Multi-epitope Vaccine.

Cross-reactivity analysis with the human proteome found no evidence of significant similarity involving the multi-epitope vaccine. This indicate a negligible risk of autoimmunity. The overall antigenicity score of 0.8317 and 0.814 by the two independent servers implemented indicate strong capacity of the vaccine to stimulate antibodies. Furthermore, allergenicity predictions using AllerTOP 2.0 and AllerFP classified the construct as non-allergenic, while toxicity analysis confirmed its non-toxic nature.

3.5. Epitope Conservancy Analysis and Homology Analysis

Epitope conservancy analysis revealed heterogeneous conservation pattern across genetically diverse Sindbis virus strains (Supplementary Table S4). The epitopes ACKARRECLT-PYAL, CTVYDRLKETTAGY, VYDRLKETTAGYITM, ERAGYAPLNLEITVMS, RAGYAPLNLEITVMSS, DMEFAQLPVNMRSEA, AYDMEFAQLPVNMRS, PRRRRQAAP-MPARNGL and WRPRRRRQAAPMPARN exhibited high levels of conservation, with approximately 70–80% of analyzed strains showing 80–100% sequence identity. This finding indicates that these epitopes are located within genetically conserved regions of the viral structural proteins. Moderate conservation (50–60%) was observed for several E1-derived epitopes, including AGPISASFTPFDHK, ISASFTPFDHKVVI, KPGAFGDIQATSLTS and PGAFGDIQATSLTSK. In contrast, a subset of E2-derived epitopes that includes CHHTVPCF-SPVKIEQV, VPCFSPVKIEQVWDE, and SYCHHTVPCFSPVKIE displayed lower conservation levels (~20%). Additionally, two capsid-derived CTL epitopes (DLPIGINITRFQTL and VVFLHVTYVPAQEK) showed no detectable conservancy across the analyzed strains. These findings indicate that the potential breadth of epitope coverage may vary among the constituent epitopes. Accordingly, the proposed multi-epitope vaccine should be regarded as a computationally prioritized candidate informed by cross-strain sequence-conservation analysis, rather than as a universally cross-protective formulation. Experimental validation is required to determine whether the selected epitopes elicit protective immune responses and to establish the extent of protection against different SINV genotypes.

3.6. Physicochemical Properties and Secondary Structure of the Vaccine Construct

Secondary structure analysis revealed the composition of 33.33 % α-helices, 13.69 % extended strands, 52.98 % random coils, and no ambiguous states (**Figure 2**). The construct has a mass number of 48.25kDa and a respective 47 and 58 negative and positive charged residues (

Table *4*). Isoelectric point score of 9.08 reflects an enrichment in basic residues which is indicative of substantial positive charge state under physiological conditions. Solubility predictions using the SoDoPE Web server yielded a solubility score of 0.7877, a flexibility value of 1.0042 and hydrophilic character score of -0.187, suggesting high solubility, moderately flexibility and favorable hydrophilicity. Additionally, half-life prediction using Protparam analysis was estimated highest in mammalian reticulocyte (~30 hours), moderate in yeast (>20 hours) and lowest in *E. coli* (> 10 hours) under in vivo conditions. With a value of 75.72, the aliphatic index reflects a thermally stable nature of the vaccine (

Table *4*)

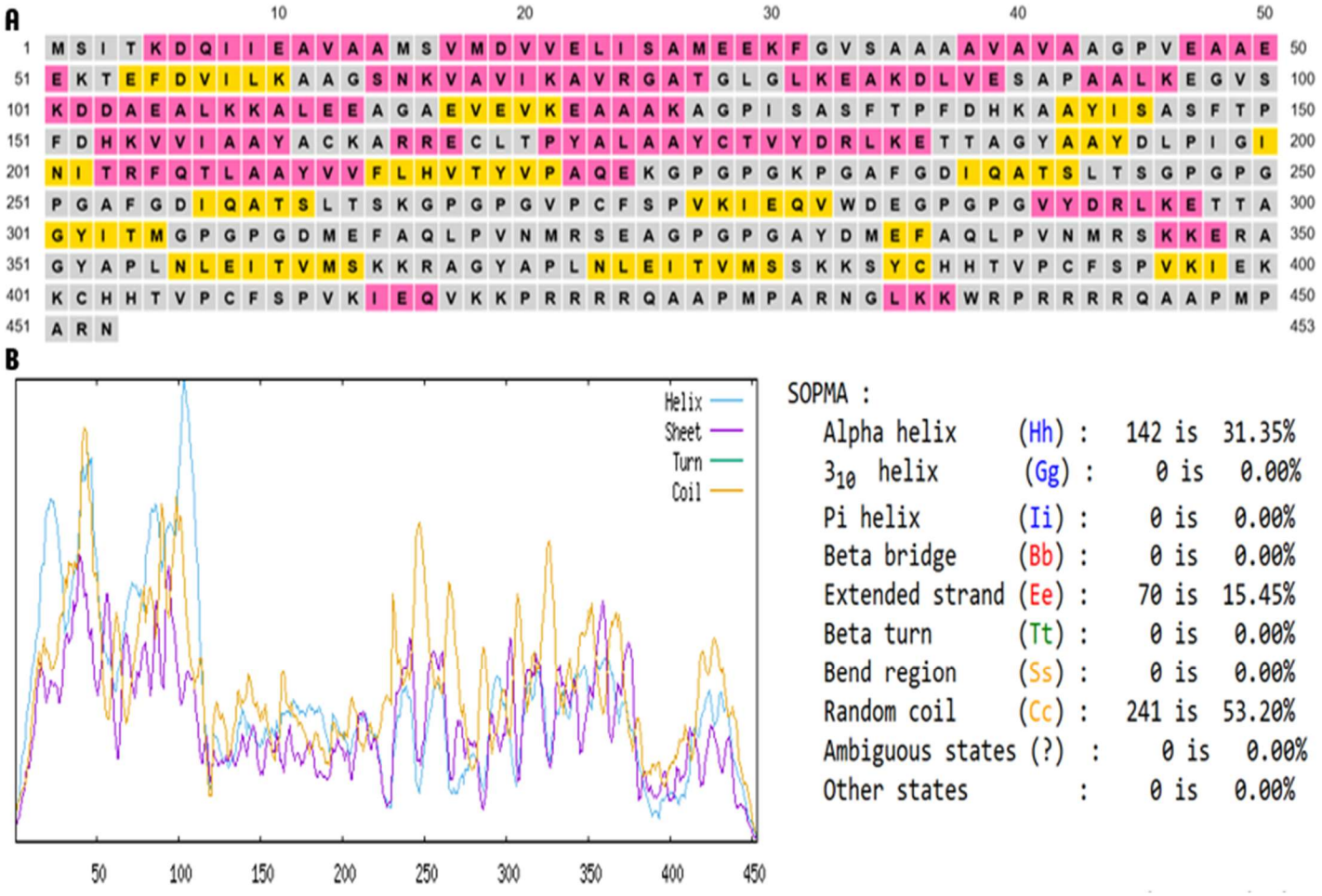


Figure 2: Composition of the vaccine construct secondary structure. (a) Representation showing helices, sheets and corresponding motifs: beta turn, gamma turn and hairpin region*s*. (b) Analysis shows 33.33 % alpha-helix, 13.69 % extended strands and 52.98 % random coils.

Table 4: Predicted physico-chemical properties of the vaccine construct.

Features	**Results**
Peptide sequence length	453
Negative charge count (Asp + Glu)	47
Positive charge count (Arg + Lys)	58
Flexibility	1.00
Theoretical pl	9.08
Aliphatic Index	75.72
Protein Stability score	55.87
Probability of Solubility	0.7877
Extinction Coefficeint	33850 m^{-1} cm^{-1}
Protein half-life estimate (In vitro)	30h

Hydrophobicity score (GRAVY)	-0.187
Formula and total number of atoms	$C_{2150}H_{3428}N_{588}O_{629}S_{21}$ (6816)

3.7. Tertiary Structure Modelling, Validation and Refinement

Among the 5 tertiary structure models predicted, the first model with the superior quality Confidence score of -2.02, Template modelling score of 0.47±0.15 and Root Mean Square Deviation value of 11.9±4.4Å was selected (**Figure 3**A). The confidence of each model is within [-5, 2], with a higher confidence towards the positive value. Template modelling and Root Mean Square Deviation scores assess the accuracy of the predicted protein structure by incorporating both prediction confidence and protein length. The global quality assessment of the vaccine construct using the QMEAN4 scoring function yielded a score of 1.10 (**Figure 3**), indicating good structural plausibility and overall model reliability.

The GalaxyRefine server which which applies iterative structure perturbation followed by overall structural relaxation to improve local geometry and side-chain conformation was further utilized to refine and optimize the structure of the vaccine. **Figure 3**, shows the analysis of the ERRAT Score plot with the overall quality factor of 78.6% and Z-score of -3.08. Proteins with approximately 400–500 amino acids have acceptable Z-scores range (−2 to −10), with higher structural reliability for values closer to zero (**Figure 3**B). The Ramachandran plot of the refined 453-amino-acid vaccine construct showed that 80.1% (301/376) of the assessed residues occupied the most favoured conformational regions, while 16.2% (61/376) were located in the additional allowed regions and 1.3% (5/376) in the generously allowed regions. The remaining 2.4% (9/376) occurred in the disallowed regions (**Figure 3**). These percentages represent the 376 non-glycine and non-proline residues included in the PROCHECK conformational-region assessment; the two

end residues, 37 glycine residues, and 38 proline residues were reported separately. The residues occupying unfavorable regions were explicitly identified as Val46, Ser261, Ile376, Pro430, Ala210, Ser16, Asp19, Phe254, and Arg432. Collectively, these complementary validation metrics provide a computational assessment of the refined model and support its use in preliminary downstream analyses, although they do not establish its experimentally determined structural accuracy.

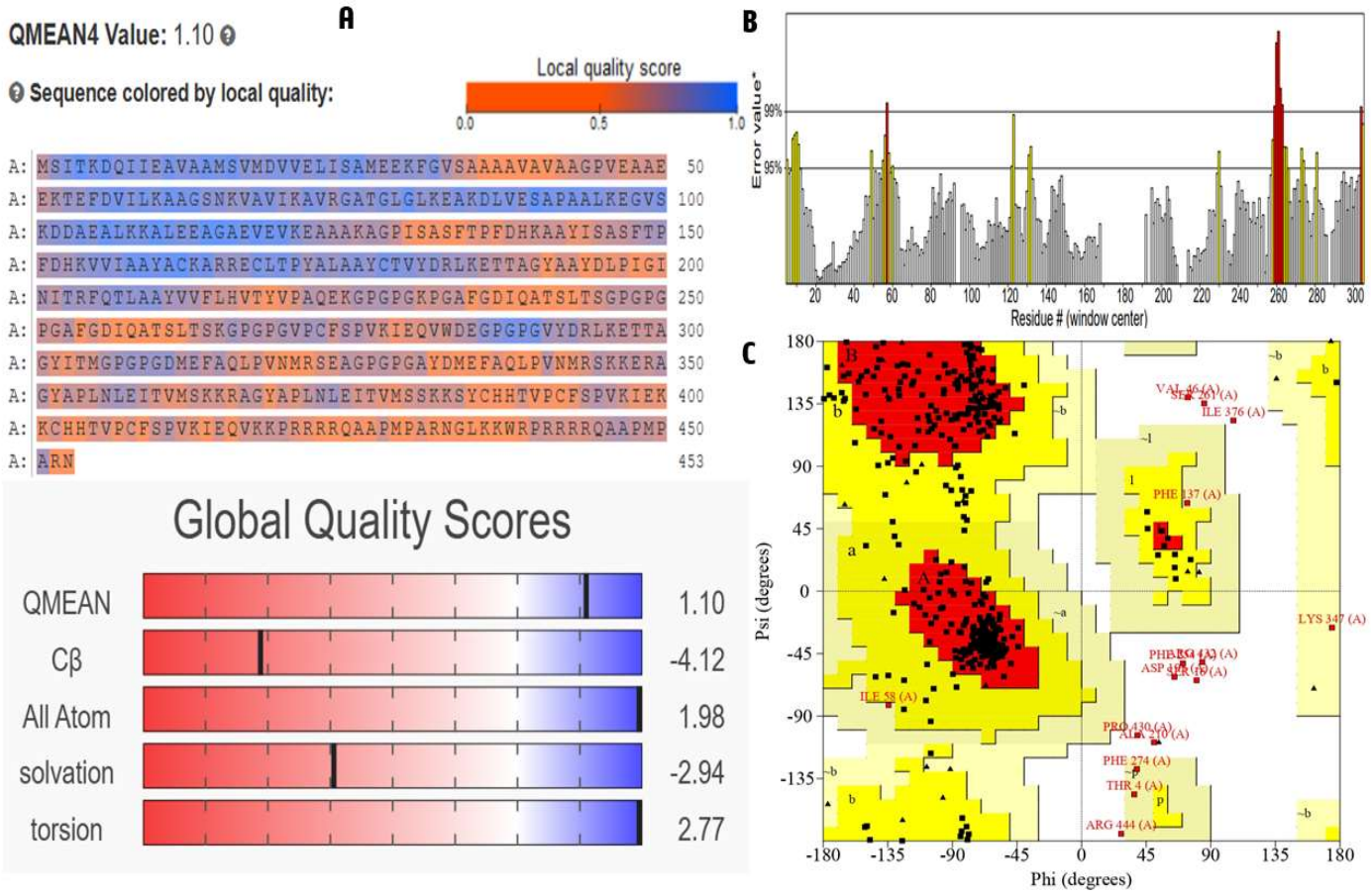


Figure 3: Vaccine Modeling and Refinement (a) QMEAN4 score of 1.10 (b) ERRAT score plot of 78.6% (c) Ramachandran plot (80.1 % residues in most favored regions, 16.2% in the additionally allowed regions, 1.3% in the generously allowed regions, and 2.4% in the disallowed regions).

3.8. Prediction of Discontinuous Epitopes

Thornton's residue clustering algorithm method through the IEDB ElliPro tool revealed the discontinuous B-cell epitopes within the vaccine [30,32]. From this analysis, five discontinuous epitopes with protrusion index score within the range of 0.5-0.8 were identified. The number of residues per epitope ranged from a minimum of 4 to a maximum of 116 residues. **Figure 4** illustrate the predicted discontinuous epitopes.

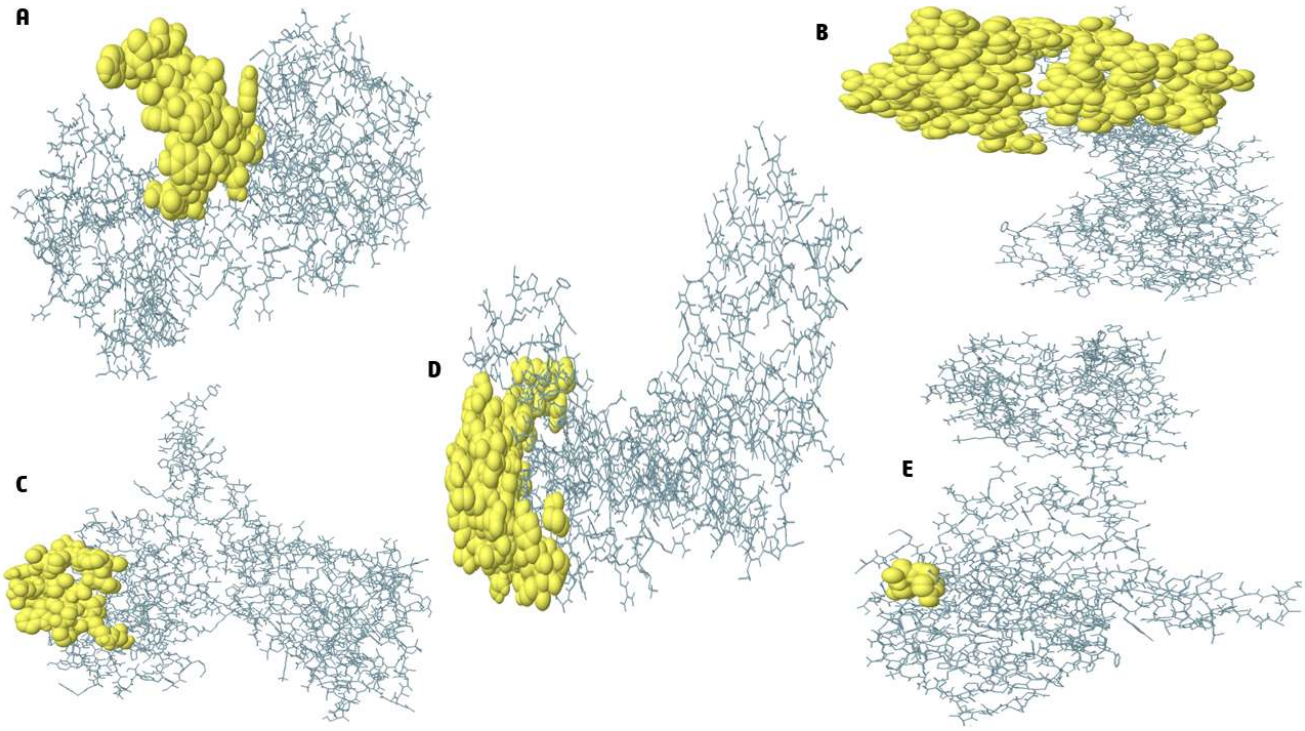


Figure 4: Discontinuous B-cell Epitopes within the vaccine construct. Epitopic residues are marked in yellow while grey shows the remaining residues. (a) 38 residues, score 0.89 (b) 116 residues, score 0.706 (c) 23 residues, score 0.65 (d) 69 residues, score 0.617 (e) 4 residues, score 0.518.

3.9. Disulfide Engineering of the Vaccine Structure

Disulfide engineering was performed to enhance the structural stability of the vaccine construct while maintaining the conformational flexibility required for effective antigen presentation. A total of 46 residue pairs were initially identified by the Disulfide by Design 2 as potential candidates

for disulfide bond formation. Only three pair of residues were found suitable for cysteine substitution after subjection to geometry screening, χ3 dihedral angle (-87° to +97°) and energy (≤ 3.0 kcal/mol). The amino acids pair showing the most favourable structural parameters of a stable and feasible disulfide bond formation were SER34–ALA37, ALA40–ALA158 and LEU372–LEU374. To be noted is the long-range interactions between ALA40 and ALA158 which could be responsible for the global stabilization of the structure and SER34-ALA37 and LEU372 LEU374 to stabilize local regions of the structure. These identified residues were mutated to cysteine to allow the formation of disulfides (**Figure 5**). All predicted residue pairs with their corresponding χ3 angles, bond energies and structural parameters is listed in the Supplementary Table S6.

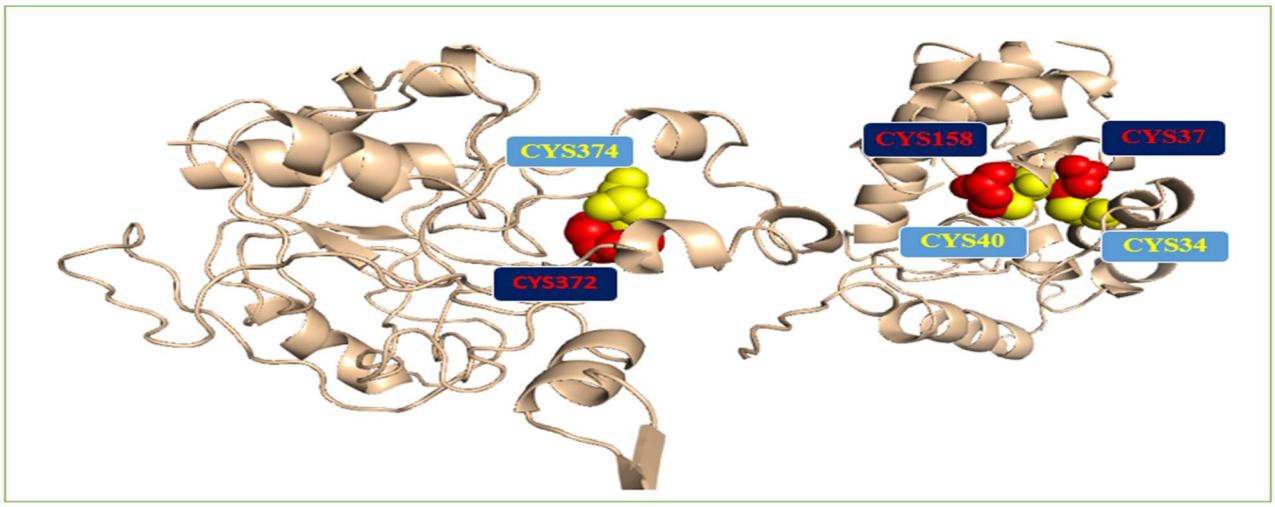


Figure 5: **Three-dimensional representation of the engineered vaccine structure showing the introduced disulfide bonds**. The selected residue pairs (SER34–ALA37, ALA40–ALA158, and LEU372–LEU374) were mutated to cysteine to facilitate disulfide bond formation, contributing to both local and global structural stabilization.

3.10. Molecular Docking Analysis

The structural compatibility represented in docking scores and the visualization of the vaccine with the adaptive (HLA-B*40:01, HLA-DRB1*07:01) and innate immune (TLR2, TLR4, TLR7 and

TLR8) receptors is showed in ***Table 5*** and ***Figure 6***/**Figure** *7*a/**Figure** *7*b respectively. In order to characterize the properties of the docked complexes, the buried surface area as well as the surface topography of the stabilizing non-covalent interactions are examined in detail in **Table 6**. The vaccine–TLR4 and vaccine–TLR7 models exhibited the largest predicted buried surface areas and highest numbers of interacting residues among the examined innate immune receptor complexes, suggesting relatively extensive modelled interaction interfaces. The predicted interfaces contained hydrogen bonds, van der Waals contacts, and ionic or salt-bridge interactions (**Figure 8**). The vaccine–TLR8 and vaccine–TLR2 models displayed comparatively smaller predicted interaction surfaces, with both hydrophobic and polar contacts (**Table 6**).

In contrast, the vaccine–HLA-B40:01 and vaccine–HLA-DRB107:01 complexes showed more localized interaction footprints, with moderate buried surface areas and fewer interacting residues. These interfaces were primarily stabilized by hydrogen bonding and hydrophobic packing, consistent with the focused binding geometry expected for peptide-presenting receptors. Hydrophobic, van der Waals force, electrostatic contact and hydrogen bond interactions which are all non-covalent in nature, exclusively mediated the interface stabilization across all the examined receptor systems. Collectively, these docking and interface analyses suggest potential structural compatibility between the vaccine construct and the selected immune receptor and MHC structures. However, these interactions remain computational predictions and do not independently establish physical binding, effective antigen presentation, or receptor activation. **Table 6Error! Reference source not found.** shows the predicted binding free energy and dissociation constant values for the vaccine-receptor complexes. PRODIGY analysis further provided estimated binding free-energy and dissociation-constant values for the modelled complexes (Table 7). Among the examined complexes, the vaccine–TLR8 model showed the most favourable predicted

binding-energy estimate (ΔG = −22.9 kcal/mol; Kd = 1.6 × 10^{-17} M), whereas the vaccine–TLR4 model showed the least favourable estimate (ΔG = −9.9 kcal/mol). While the docking score from the Cluspro server is further supported by the PRODIGY tool, these values represent only computational estimates and should not be interpreted as experimentally measured binding affinities.

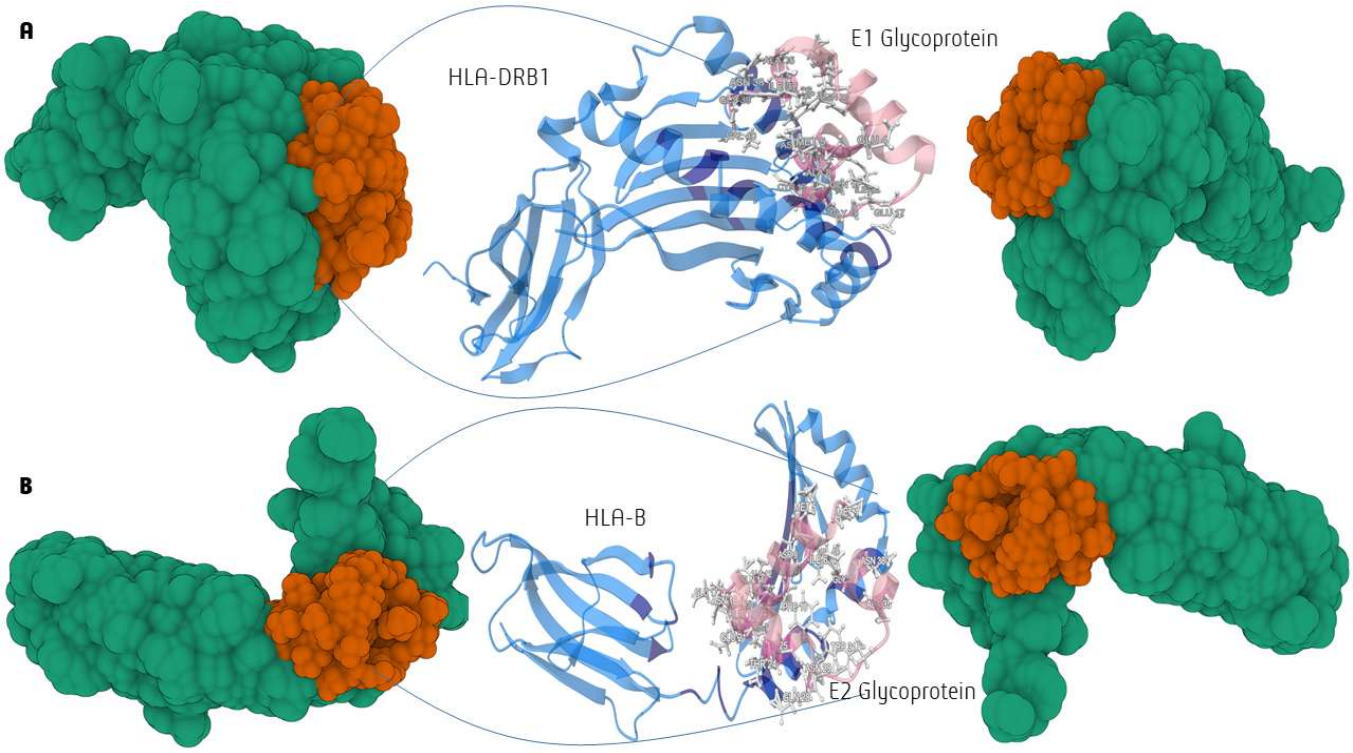


Figure 6: Docking representations illustrating the binding of vaccine epitopes to HLA receptors. The epitopes are indicated in hot pink/blue; HLA receptors are shown in lime green. (a) Complex of E1 (KPGAFGDIQATSLTS) with HLA-DBR1*07:01 (b) Complex of E2 (ACKARRECLTPYAL) with HLA-B*40:0.

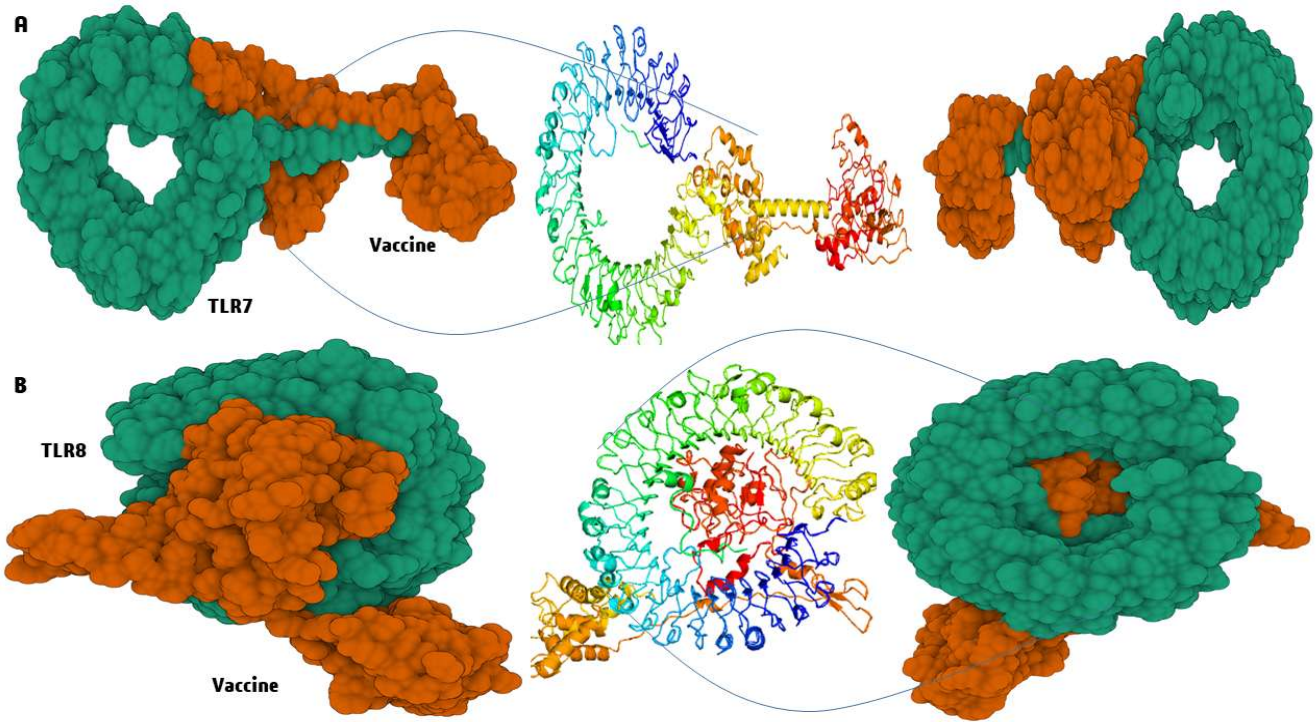


Figure 7a: Docking model of the binding interaction of vaccine with TLR7/TLR8 molecule. (a) TLR7 and vaccine complex. (b) TLR8 molecule and vaccine complex.

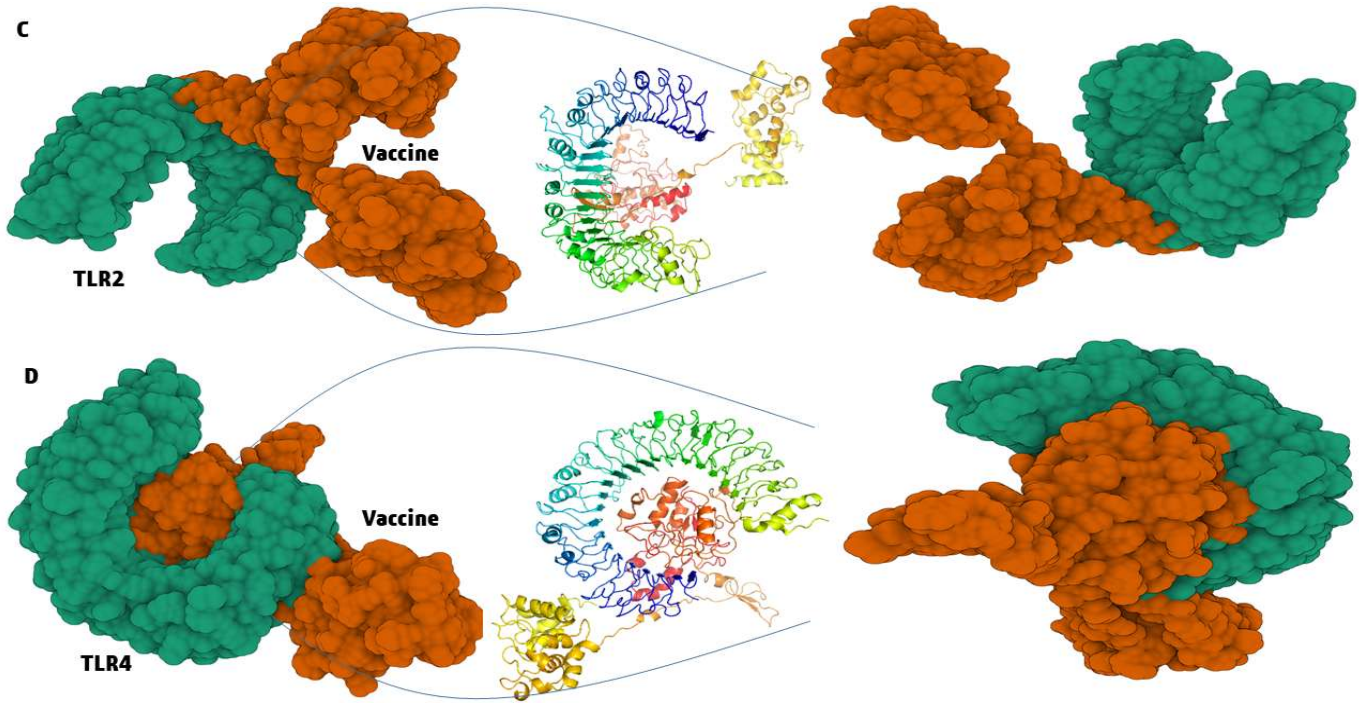


Figure 7b: Docking model of the binding interaction of vaccine with TLR2/TLR4 molecule. (a) TLR2 and vaccine complex. (b) TLR4 molecule and vaccine complex.

Table 5: Result of Molecular Docking

Parameters	**Vaccine-HLA-B*40:01**	**Vaccine-HLA-DRB1*07:01**	**Vaccine-TLR2**	**Vaccine-TLR4**	**Vaccine-TLR7**	**Vaccine-TLR8**
Center Weighted Score	−640.6	−838.7	−999.0	−1188.0	−1117.9	−1125.0
Lowest Energy Score	−850.0	−929.7	−1180.0	−1311.4	−1395.0	-1285.8
Electrostatic Favored	−896.0	−962.2	−1343.2	−1255.4	−1453.3	-1526.7
Hydrophobic-favored	−1058.4	−428.3	−1944.8	−1599.4	−2156.9	-1581.8
Van der Waals +Electrostatic	−164.7	−148.8	−321.6	−346.7	−445.3	-415.6

Table 6: Interface Properties and Predicted Binding Affinity of Vaccine-Receptor Complexes

Parameters	**Vaccine-HLA-B*40:01**	**Vaccine-HLA-DRB1*07:01**	**Vaccine-TLR2**	**Vaccine-TLR4**	**Vaccine-TLR7**	**Vaccine-TLR8**
Predicted Binding affinity (ΔG) (kcal/mol)	−10.2	-10.5	-9.9	−20.3	-15.8	-22.9
Dissociation Constant (Kd)	3.4e-08	2.1e-8	5.2e-08	1.3e-15	2.5e-12	1.6e-17
Buried Surface Area (Å²)	2017.8	1860.5	2333.2	5102.3	5061.6	4198.9
Polar (%)	37.1	41.4	23.78	38.21	45.2	30.2
Non-Polar (%)	62.9	58.7	76.22	61.79	54.8	69.8
Number of H−Bonds	11	13	7	22	22	14
Number of Salt Bridges	2	1	0	9	10	3
Apolar vdW Contacts	13	16	73	25	16	38
CH–O/N bonds	10	19	16	19	19	23
(π–π + CH–π)	1	5	5	8	9	2
Total Interacting Residues	43	49	59	135	144	107

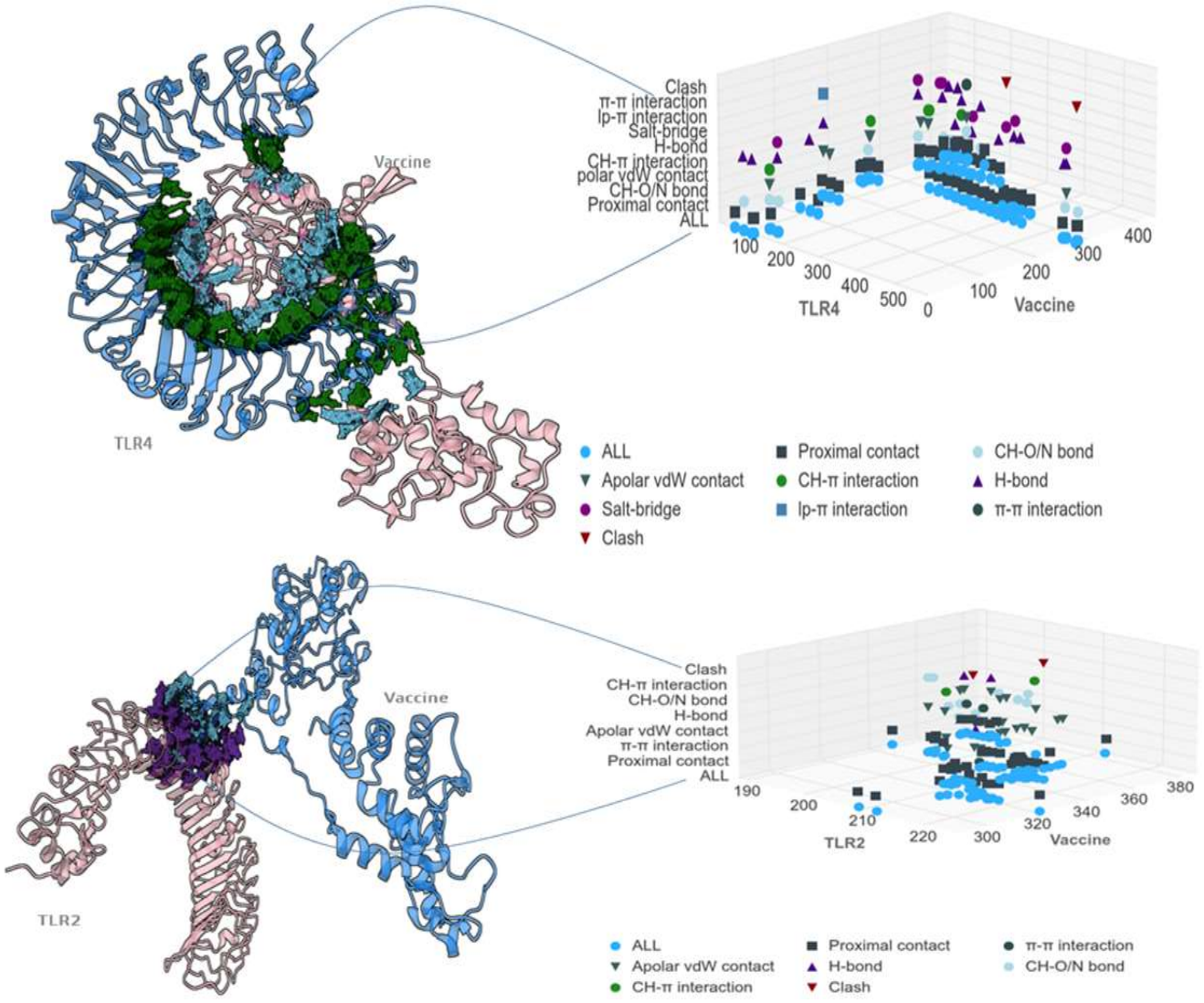


Figure 8: Atomic Interaction 3D Contact Map of TLR2/TLR4 Vaccine Complexes

3.11. Normal Mode Analysis

Normal Mode Analysis of the unbound receptor models and their corresponding vaccine–receptor complexes revealed receptor-specific differences in the predicted structural flexibility and deformation characteristics (**Figure 9** and **Figure *10***). The eigenvalue, which reflects the resistance of the structure to deformation, was used as a comparative metric. Residue deformability analysis illustrates the flexibility and rigidity of individual residues along the protein chain, with

values ranging from 0 and 1 Å. The eigenvalue for TLR2 decreased from 1.13×10^{-5} to 9.21×10^{-7}, suggesting a lower resistance to deformation in the modelled complex. TLR7 showed a comparatively smaller change in eigenvalue, from 3.31×10^{-6} to 1.69×10^{-6}. In contrast, the eigenvalue for TLR4 increased from 1.24×10^{-5} to 2.19×10^{-5}, indicating greater resistance to deformation in the corresponding model, while that of TLR8 decreased from 1.01×10^{-4} to 2.05×10^{-5}. These differences provide insights into the predicted collective motions and conformational flexibility of the modelled receptor–vaccine complexes. However, the NMA results do not establish the occurrence or stability of these interactions under physiological conditions.

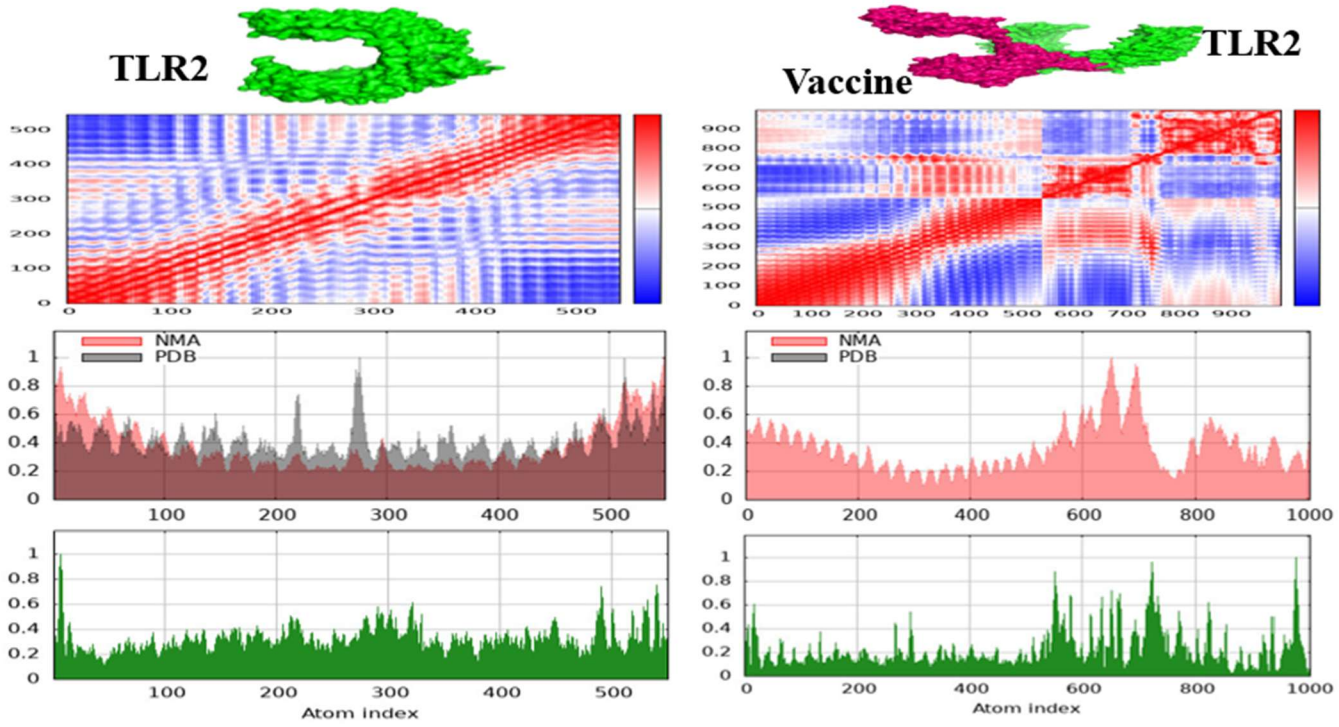


Figure 9: Normal Mode Analysis of unbound receptors TLR2 and receptor–vaccine complexes. (A) Covariance Analysis of Atomic Fluctuations (B) B-factor (C) Deformability map.

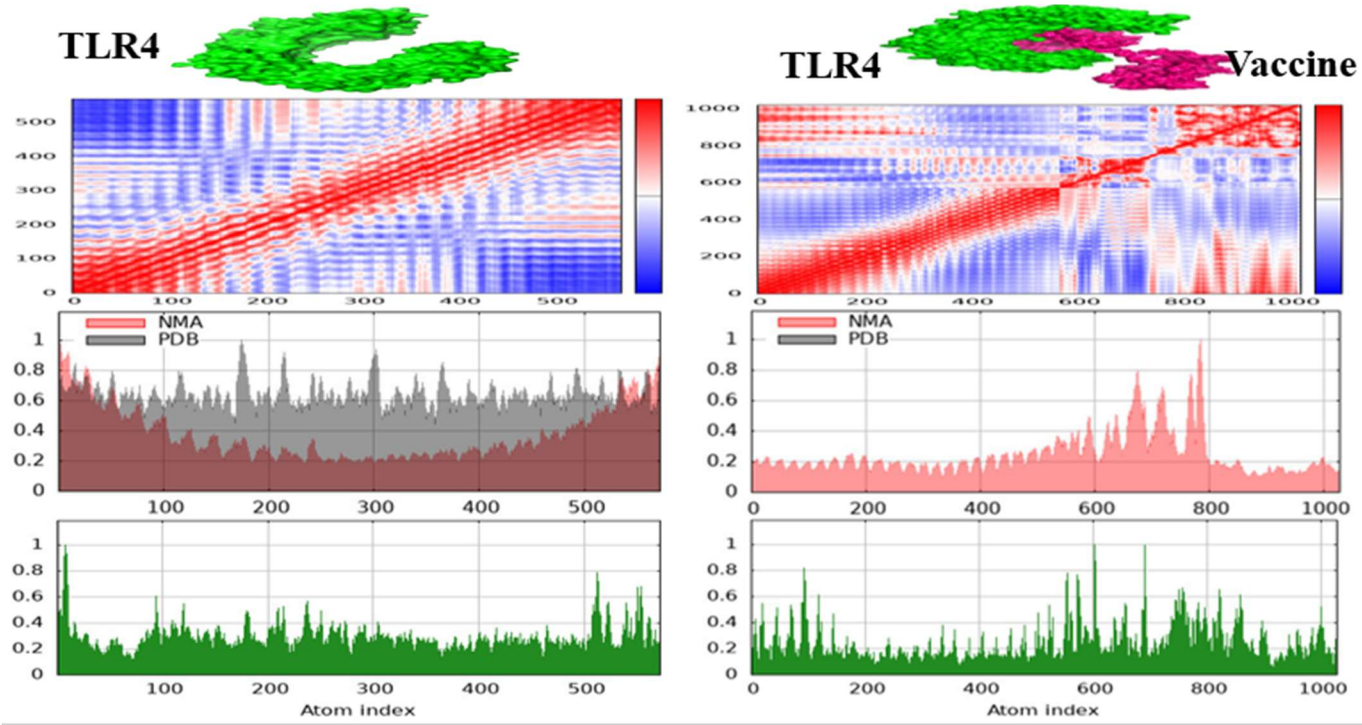


Figure 10: Normal Mode Analysis of unbound receptors TLR4 and receptor–vaccine complexes. (A) Covariance Analysis of Atomic Fluctuations (B) B-factor (C) Deformability map.

3.12. *In silico* Immune Simulation

The predicted immune-response profiles generated by C-ImmSim over a 35-day period following a single simulated vaccine administration are presented in **Figure 11** and **Figure 12**. The simulation indicated increased IL-2 and IFN-γ levels, alongside a progressive rise in antibody titres, which reached approximately 14,000 units before declining slightly to about 12,000 units by day 15. An increase in the simulated plasma-cell population was observed from day 3, together with sustained memory-cell representation (**Figure 11** and **Figure 12**). Both activated and resting helper T-cell populations showed an increasing trend from day 5, reaching a plateau around day 12. The simulated cytotoxic T-lymphocyte population also increased throughout the simulation period. In addition, the model predicted changes in natural killer-cell, macrophage, and dendritic-cell populations. Natural killer-cell representation decreased briefly between days 15 and 20 before increasing subsequently, whereas the dendritic-cell and macrophage profiles remained relatively stable during the simulated period (Figure 12). These outputs represent computationally predicted immune-response patterns and do not establish that the vaccine will induce equivalent responses in vivo (**Figure 12**).

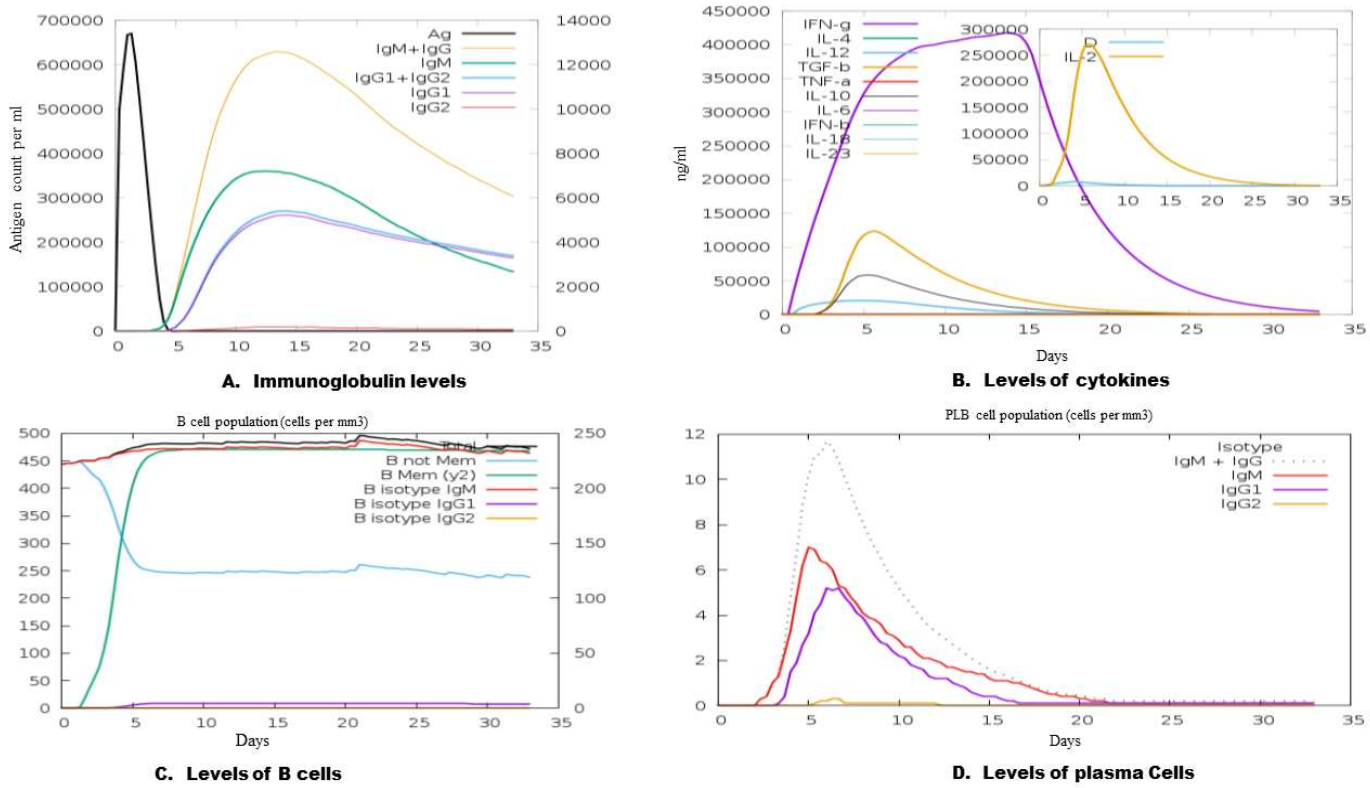


Figure 11: Immune response analysis showing activation patterns of innate and adaptive cellular components subsequent to vaccine exposure.

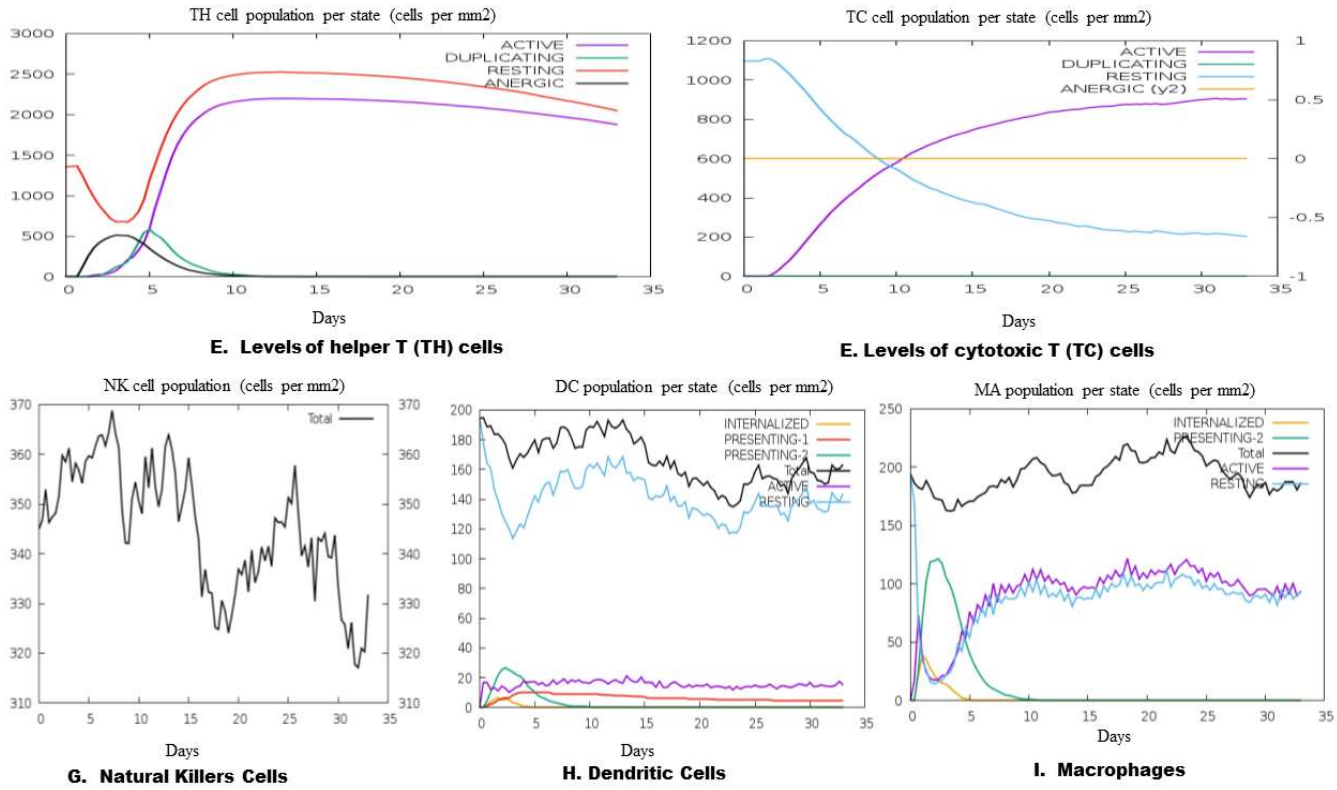


Figure 12: Immune response analysis showing activation patterns of innate and adaptive cellular components subsequent to vaccine exposure.

3.13. Condon Optimization and *In silico* cloning

Translation and optimization of the vaccines proteomic sequence into genomic sequence resulted to a total number of 1,350 bp cDNA fragment with Adaptation Index and Guanine-Cytosine (GC) content of 0.94 and 52.17% respectively. Optimal DNA sequence have a codon adaptation above 0.8 and GC content between 30% and 70 % [45]. *In silico* restriction mapping confirms the feasible insertion of this fragment into the pYES2(+) vector (**Figure 13**), demonstrating its compatibility with standard *Saccharomyces cerevisiae* expression systems.

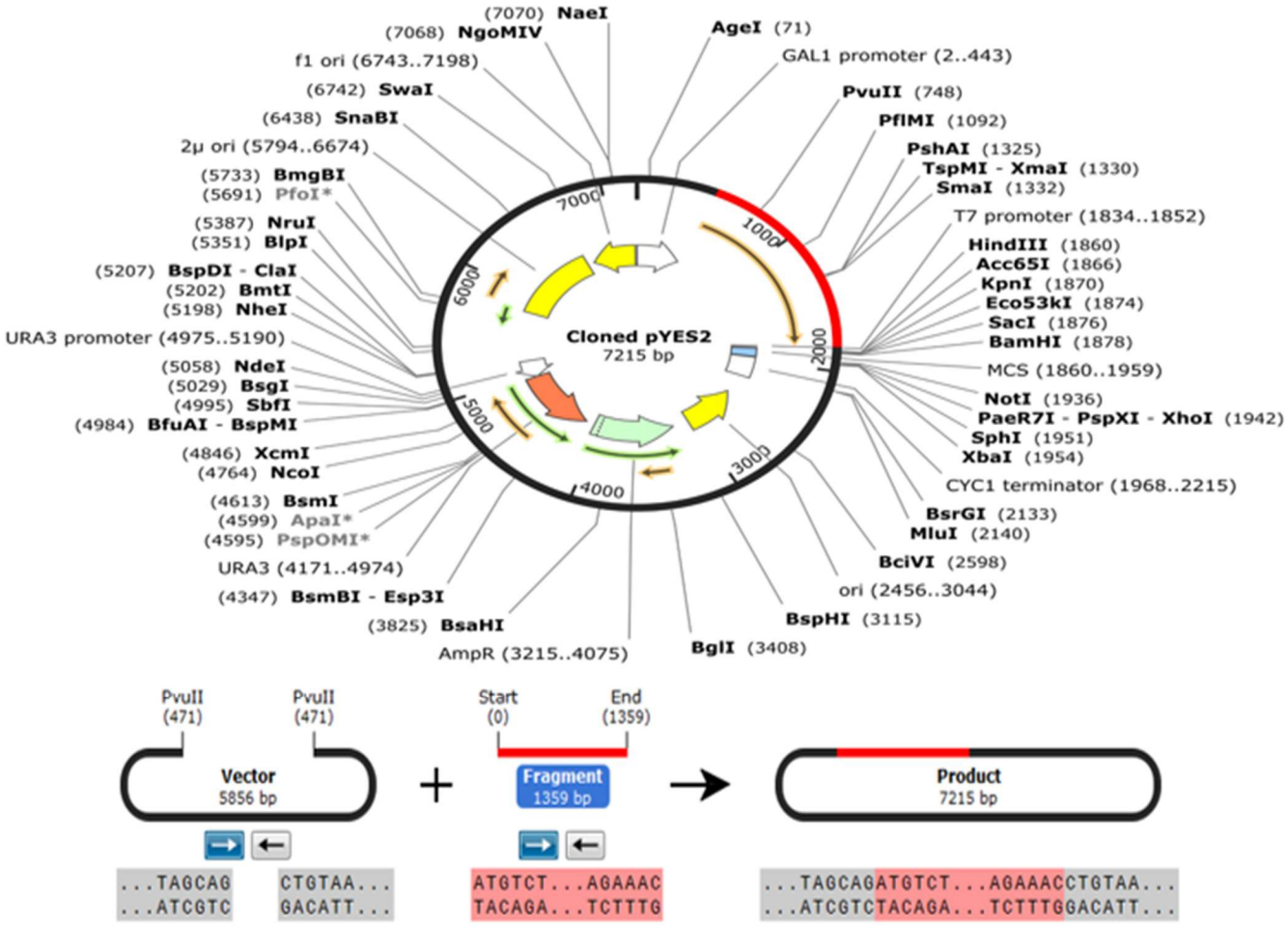


Figure 13: *In silico* modeling of recombinant plasmid design showing the vaccine sequence (orange) integrated within the pYES2 (+) vector at the PvuII restriction site.

4. Discussion

Reverse vaccinology connotes the use of a pathogen's genetic information as the foundation for design vaccine rather than relying on the organism itself [30,46]. Since its first successful application by [47], to identify suitable vaccine candidates against Serogroup B meningococcus, this approach has remained a reliable technology for antigen discovery. Among its many applications, the techniques has been successfully deplored to design vaccines against several viruses that include Dengue, Ebola and Avian influenza virus [15,48–50]. Notably, it took only two months of World Health Organization's designation of COVID-19 as a global health emergency in 2020, for computationally designed vaccine candidates to appear in peer-reviewed literatures.

Recurrent epidemics of SINV infection in Northern European countries and South Africa have been documented, with genotype I strain of the virus being most frequently associated with human disease outbreaks [5,6]. Although wild birds serve as the natural reservoir and amplifying host of the virus, humans develop arthritogenic and febrific symptoms following bites from infected mosquito vectors. According to [6], the disease has remained underdiagnosed, poorly understood and the full burden in terms of its febrile and neurological manifestations remains inadequately characterized. To date, no specific antiviral therapies exist and clinical management focuses on symptom relief rather than addressing the underlying viral infection [8].

This study demonstrates the feasibility of a rationally designed multi-epitope vaccine targeting structurally exposed and immunologically relevant regions of the Sindbis virus proteome. The vaccine construct is designed to target the readily accessible envelope glycoproteins E1, E2, and capsid protein which are known to aid in viral attachment, membrane fusion and assembly. The choice of this design is guided by the Sindbis virus genome organisation, where Open Reading

Frame (ORF2) constitutes both the virion architecture and the primary targets of host immune recognition [16]. Importantly, the exclusion of the E3 glycoprotein is related to its low relevance in the mature virions, as this glycoprotein is cleaved during viral processing [16]. Likewise, the non-structural proteins (nsP1–nsP4) have been described to contain T-cell epitopes, but since they are not associated with the virion surface architecture or involved in virion assembly, they do not directly contribute to antibody neutralisation [51]. This antigen selection strategy increases the chances of inducing both humoral and cellular immune responses by targeting structurally and functionally relevant viral determinants.

The predicted sequences were carefully analysed to derive a finalised multi-epitope vaccine construct which included eighteen epitopes consisting of six CTL, HTL and B-cell epitopes each. Their assembly was designed following the description format of [30], where linker sequences were strategically utilised to optimise antigen processing and presentation. In particular, the rigid EAAAK linker was utilised to separate the epitope and adjuvant regions while maintaining their functional independence. The AAY linker was added to ensure proteasomal degradation and efficient presentation on MHC class I molecules. The GPGPG linker was added to ensure efficient MHC class II processing, while KK linkers were incorporated to increase the accessibility of B-cell epitopes for humoral immune recognition. Consistent with previous multi-epitope vaccine designs by [52,53], the immunostimulatory N-terminal region of the 50S ribosomal protein L7/L12 was chosen because of its ability to stimulate general immune activation.

The similarity of the amino acid sequence of the vaccine construct, as determined by Protein Basic Local Alignment Search Tool (BLASTp) evaluation, showed no significant homology to the human proteome, suggesting a low potential for autoimmune cross-reactivity. The antigenicity score of 0.8317, in combination with allergenicity and toxicity assessments using AllerTOP 2.0,

AllerFP, and ToxinPred 2.0 servers, identified the vaccine construct to be antigenic, non-allergenic and non-toxic. In line with [54], the vaccine construct's molecular weight of 48.25 kDa is considered suitable for expression and subsequent purification of recombinant proteins in bacteria. The isoelectric point of 9.08 indicates a positive charge at neutral pH, similar to what was observed in similar MEV studies on influenza virus [55]. The vaccine construct exhibited a predicted solubility score of 0.7877, flexibility index of 1.0042, and hydropathicity value of −0.187, suggesting potentially favourable solubility and moderate flexibility. The predicted half-life lies within the acceptable range of 30 hours, while the instability index of 55.87 exceeded the conventional threshold of 40, indicating a potential tendency towards protein instability based on its amino acid composition [56]. However, this sequence-based estimate does not establish actual protein degradation, expression yield, or storage stability. Experimental assessment will therefore be necessary to determine the stability of the expressed construct under relevant conditions. If instability is confirmed, formulation approaches involving stabilizing excipients, such as sucrose or trehalose, and nanoparticle-based delivery systems may be investigated to improve antigen integrity [57–59]. Their effectiveness would likewise require experimental evaluation.

The three-dimensional structural assessment provided complementary computational estimates of the quality of the predicted vaccine model. The I-TASSER confidence score of −2.02 and TM-score of 0.47 ± 0.15 provided an indication of the model's prediction confidence and structural similarity, respectively. Further assessment yielded a ProSA Z-score of −3.08, an ERRAT quality factor of 78.6%, and a QMEAN4 score of 1.10, collectively providing additional information on the model's global structural characteristics. Ramachandran plot analysis showed that 80.1% of the assessed residues occupied the most favoured regions, while 16.2% and 1.3% were located in the additional and generously allowed regions, respectively. The remaining 2.4% occurred in

disallowed regions, indicating localized stereochemical limitations. Targeted loop modeling, where structurally appropriate, followed by energy minimization and stereochemical revalidation, could potentially improve these regions. For further structural stability, the conformational integrity of the vaccine construct was reinforced through three pairs of residues selected for disulfide engineering: SER34–ALA37, ALA40–ALA158, and LEU372–LEU374. The incorporation of these covalent bonds is expected to decrease local structural fluctuations while maintaining the flexibility required for antigen presentation. [45, 49] reported the use of similar stabilisation strategies to enhance the structural resistance of their multi-epitope vaccine constructs without affecting their immunogenic properties.

In keeping with this structural optimisation, molecular docking revealed good binding interactions between the vaccine construct and Toll-like receptors. The predicted binding affinities of the TLR8 ($\Delta G = -22.9$ kcal/mol) and TLR4 ($\Delta G = -20.3$ kcal/mol) complexes suggest strong and stable interactions. Binding affinities were comparatively lower for TLR2 and TLR7 but remained within the range indicative of receptor–ligand interaction. Interestingly, the binding affinity values derived for both TLR4 and TLR8 were found to be similar to those reported in related multi-epitope vaccine investigations, such as [53], who reported binding energies for TLR4 and TLR8 within a similar range (−23.35 kcal/mol). Investigating further into the stability and flexibility of these interactions through comparative Normal Mode Analysis showed that vaccine binding causes receptor-specific changes in structural dynamics. While the increased rigidity observed in TLR4 could indicate stabilisation of the complex, the observed flexibility in the TLR2 and TLR8 receptors may indicate the adaptability of these receptors to the conformation of the ligand. Such variations may reflect differences in the predicted flexibility of the docked receptor–construct complexes. However, these observations are derived from Normal Mode Analysis (NMA), which

uses simplified harmonic approximations to describe collective motions around a modeled structure. Although NMA can provide insights into intrinsic flexibility and relative patterns of motion, it does not fully represent explicit-solvent effects, unrestricted atomic-level dynamics, or large-scale conformational rearrangements occurring over longer timescales. Accordingly, the observed differences in flexibility should be interpreted as model-dependent predictions rather than definitive evidence of complex stability or functional receptor engagement.

Although the molecular docking suggested favorable structural interaction with TLR7 and TLR8, it is important to emphasize that these receptors are endosomal sensors of single-stranded RNA rather than classical protein ligands. Therefore, the docking analyses should be interpreted as structural interaction assessments rather than evidence of direct ligand-receptor engagement or signaling activation. In a physiological context, innate immune activation would more plausibly occur indirectly through antigen internalization by antigen-presenting cells, followed by endosomal processing and downstream pattern-recognition signaling. The immune simulation analysis following vaccine administration revealed strong IFN-γ, IL-2 induction coupled with dendritic, macrophages and natural killer cells activation. The rise in innate immune cell population will contribute to early viral clearance and cytokine production.

The inclusion of epitopes with different conservation profiles reflects the diversity observed among the analyzed strains; however, the potential breadth of epitope coverage cannot be inferred from sequence conservation alone. Accordingly, the proposed vaccine should be regarded as a computationally prioritized candidate informed by cross-strain sequence-conservation analysis, rather than as a formulation demonstrated to provide universal cross-genotypic protection. The inclusion of different epitopes in the vaccine construct was intended to support both antibody-mediated and T-cell-mediated immune responses. Neutralizing antibodies that block viral entry,

together with cytotoxic T lymphocytes that eliminate infected host cells, represent complementary mechanisms potentially involved in protection against alphavirus infection. Consistent with this immunological rationale, our in silico immune simulation predicted antibody responses alongside cellular immune profiles characterized by IFN-γ-associated signatures, suggesting the potential to stimulate complementary humoral and cellular responses. Nevertheless, these simulated profiles do not demonstrate that the proposed construct will elicit equivalent immune responses in vivo or confer protection against SINV infection. The ability of the predicted responses to mediate viral clearance or prevent chronic arthralgic manifestations therefore remains to be established experimentally. Chronic arthralgia following alphavirus infections is believed to involve a complex interplay of viral persistence and immune-mediated pathology. Although immune activation is an intended outcome of vaccination, excessive or dysregulated inflammation could theoretically contribute to immunopathology. SINV-associated arthralgia has been linked to pro-inflammatory responses, including cytokine release and pathways associated with joint tissue damage [3,60]. However, whether the proposed epitope-based construct could exacerbate such pathology remains unknown and cannot be determined from the present computational analyses. Equally, whether immune responses induced by the proposed vaccine could prevent acute infection or mitigate chronic arthralgic sequelae must therefore be established experimentally. Computational predictions alone cannot resolve these outcomes. Further experimental studies are needed to determine whether the predicted immunological responses translate into functional protection and whether vaccination has any effect on chronic disease manifestations.

4.1. Potential Limitation of the Study

This study is entirely computational and does not include experimental validation. Consequently, the immunogenicity, protective efficacy, and durability of immune responses induced by the

proposed multi-epitope vaccine remain inferential until confirmed through experimental studies. Molecular docking provides estimates of potential molecular interactions based on modelled structures and the assumptions of the docking protocol; however, it does not independently establish physical binding, receptor activation, or biological function. Similarly, Normal Mode Analysis (NMA) characterizes collective motions using simplified harmonic approximations around a modeled structure. These approximations do not fully capture explicit-solvent dynamics, unrestricted atomic-level movements, or large-scale conformational changes occurring over extended timescales. Therefore, the docking and NMA findings should be regarded as preliminary structural predictions rather than definitive evidence of stable complexes or functional interactions. Although C-ImmSim provides insights into possible immune-response patterns, it cannot fully reproduce the complexity of antigen processing, presentation, host immune regulation, or potential immunopathological responses in biological systems. Further investigation using explicit-solvent molecular dynamics simulations, where appropriate, together with experimental binding and functional assays, would help evaluate the predicted interactions more comprehensively. Additional studies, including peptide–MHC binding assays, T-cell activation assays, antigen-presenting cell uptake studies, and in vivo immunogenicity and protection studies, would also be necessary to assess the biological relevance, safety, and protective potential of the proposed construct.

Despite the aforementioned limitations, the study provides a scientifically grounded framework for rational epitope prioritization for va7ccine design. While this work should be viewed as an essential step toward the development of vaccine against SINV infection, future studies should validate the immunogenicity of the epitope, assess their long-term immune memory and evaluate their protective efficacy in relevant biological models.

5. Conclusions

This study presents a computationally designed multi-epitope vaccine candidate targeting the E1, E2, and capsid proteins of Sindbis virus (SINV). The computational analyses provide preliminary evidence of predicted structural compatibility, conformational flexibility, and potential humoral and cellular immune responses. However, these findings remain predictive and do not establish the vaccine's actual immunogenicity, safety, or protective efficacy. Further experimental validation, including in vitro binding assays, cell-uptake studies, immune-cell activation assays, and in vivo safety and challenge studies, is therefore essential to establish the biological relevance and suitability of the proposed construct as a vaccine candidate against SINV infection.

List of Abbreviations

SINV: Sindbis virus

MEV: Multi-epitope vaccine

TLR: Toll-like Receptor

MHC: Major Histocompatibility Complex

QMEAN: Qualitative Model Energy Analysis,

nsP1: non-structural proteins 1

IRAK1: Interleukin-1 Receptor-Associated Kinase 1

CTL: Cytotoxic T Lymphocyte

HTL: Helper T Lymphocyte

B-cell: B lymphocyte

HLA: Human Leukocyte Antigen

IL-2: Interleukin-2

IFN-γ: Interferon-gamma

DNA: Deoxyribonucleic acid

RNA: Ribonucleic acid

GC: Guanine-Cytosine

PI: Isoelectric Point

RMSD: Root-Mean-Square Deviation

TM-score: Template Modeling score

PSI-BLAST: Position-Specific Iterative Basic Local Alignment Search Tool

BLASTp: Protein Basic Local Alignment Search Tool

DPC: Dipeptide Composition

TH: T helper cell

NKC: Natural Killer cell

ORF: Open Reading Frame

Supplementary Materials:

S1 Table: Supplementary Table S1__Full CTL Epitope Prediction Outputs;

S2 Table: Supplementary Table S2__Full HTL Epitope Prediction Outputs;

S3 Table: Supplementary Table S3__Full B-Cell Epitope Prediction Outputs;

S4 Table: Supplementary Table S4__Epitope Conservancy Result

S5 Table: Supplementary Table S5__ HTL Epitopes and their cytokines properties.

S6 Table: Supplementary Table S6__ Disulfide Engineering Result analysis

Author contributions Statement

E.O.A. (Emmanuel Oladiran Amos): Conceptualization, Methodology, Data curation, Formal analysis, Visualization, Project administration, Writing—original draft preparation. O.S.A.: Methodology, Investigation, Resources, Writing—review and editing. S.O.A.: Validation, Formal analysis, Investigation, Visualization, Supervision, Writing—review and editing. E.O.A. (Enoch Olanrewaju Akinleye): Data curation, Validation, Visualization, Writing—review and editing. O.O.O.: Resources, Visualization, Writing—review and editing. J.F.S.: Validation, Data curation, Project administration, Writing—review and editing. O.M.K.: Supervision, Resources, Validation, Writing—review and editing. All authors have read and agreed to the published version of the manuscript.

Data Availability Statement

All datasets supporting the conclusions of this study are openly available in the UniProt database at https://www.uniprot.org/ under the accession numbers UP000006710 and UniRef100_UPI0005A61EDB, and in the National Center for Biotechnology Information (NCBI) database at https://www.ncbi.nlm.nih.gov/ under the accession numbers NC_001547.1, AF429428.1, AF103728.1, OK491658.1, MH212167.1, M69205, AF103734, U38305, PP889333, and J02363.1.

Conflicts of Interests

The authors declare that they have no conflicts of interest to this work.

Funding

The authors received no funding for this work.

Acknowledgements

Declared none.

AI Declaration:

ChatGPT (GPT-6) was used in some portions of the manuscript solely for language editing, formatting, and grammatical adjustments to improve readability and comprehension of the scientific text. The authors critically reviewed all suggested modifications and take full responsibility for the accuracy, originality, and integrity of the work.

References

[1] Strauss JH, Strauss EG. The alphaviruses: gene expression, replication, and evolution. Microbiol Rev 1994;58:491–562. https://doi.org/10.1128/mr.58.3.491-562.1994.

[2] Ling J, Smura T, Lundström JO, Pettersson JH-O, Sironen T, Vapalahti O, et al. Introduction and Dispersal of Sindbis Virus from Central Africa to Europe. J Virol 2019;93:e00620-19. https://doi.org/10.1128/JVI.00620-19.

[3] Sokoloski KJ, Karki D, Isom CM, Moni S. The pathogenicity and virulence of Sindbis virus. Virulence 2026;17:2609389. https://doi.org/10.1080/21505594.2025.2609389.

[4] Kim AS, Diamond MS. A molecular understanding of alphavirus entry and antibody protection. Nat Rev Microbiol 2023;21:396–407. https://doi.org/10.1038/s41579-022-00825-7.

[5] Matthew DA, Karlsson E, Izang JA, Isberg L, Näslund J, Sjödin A, et al. First detection of Sindbis virus in wild birds in Nigeria. Sci Rep 2025;15:24621. https://doi.org/10.1038/s41598-025-10556-3.

[6] Meno K, Yah C, Mendes A, Venter M. Incidence of Sindbis Virus in Hospitalized Patients With Acute Fevers of Unknown Cause in South Africa, 2019–2020. Front Microbiol 2022;12:798810. https://doi.org/10.3389/fmicb.2021.798810.

[7] Gutiérrez-López R, Ruiz-López MJ, Ledesma J, Magallanes S, Nieto C, Ruiz S, et al. First isolation of the Sindbis virus in mosquitoes from southwestern Spain reveals a new recent

introduction from Africa. One Health 2025;20:100947. https://doi.org/10.1016/j.onehlt.2024.100947.
[8] Harding S, Sewgobind S, Johnson N. JMM Profile: Sindbis virus, a cause of febrile illness and arthralgia: This article is part of the JMM Profiles collection. Journal of Medical Microbiology 2023;72. https://doi.org/10.1099/jmm.0.001674.
[9] Suvanto MT, Uusitalo R, Otte Im Kampe E, Vuorinen T, Kurkela S, Vapalahti O, et al. Sindbis virus outbreak and evidence for geographical expansion in Finland, 2021. Eurosurveillance 2022;27. https://doi.org/10.2807/1560-7917.ES.2022.27.31.2200580.
[10] Jagdev M, Parekh I, Bruce RC, Spiro S, Johnston CJ, Abbott AJ, et al. Enhanced surveillance to assess the presence of Sindbis and Batai virus in mosquito populations at an urban zoo in the United Kingdom. Parasites Vectors 2025. https://doi.org/10.1186/s13071-025-07149-4.
[11] Kaboré DPA, Exbrayat A, Charriat F, Soma DD, Sawadogo SP, Ouédraogo GA, et al. A metagenomics survey of viral diversity in mosquito vectors allows the first detection of Sindbis virus in Burkina Faso. PLoS One 2025;20:e0323767. https://doi.org/10.1371/journal.pone.0323767.
[12] Sant'Anna MW, Ferreira ML, Da Silva LF, Côrtes PL. Climate Change and Arbovirus: A Review and Bibliometric Analysis. Climate 2025;13:35. https://doi.org/10.3390/cli13020035.
[13] Papa A. Emerging Arboviruses in Europe. AMH 2024;69:322–37. https://doi.org/10.3390/amh69040029.
[14] Ira NI, Jaishee N, Saha A, Naidoo D, Islam ST, Tani TH, et al. Development of a multi-epitope vaccine candidate against Sindbis virus through integrated immunoinformatics approaches and molecular dynamics simulations. Computers in Biology and Medicine 2026;202:111456. https://doi.org/10.1016/j.compbiomed.2026.111456.
[15] Amos EO, Araoyinbo OS, Akinleye EO, Alakanse SO, Bamikole AO, Kolawole OM. Immunoinformatics design of multi-epitope vaccine using surface cell antigen OmpB and heat shock protein GroEL against rickettsioses. Informatics in Medicine Unlocked 2023;43:101411. https://doi.org/10.1016/j.imu.2023.101411.
[16] Geng Q, Navaratnarajah CK, Zhang W. Structural and Functional Hallmarks of Sindbis Virus Proteins: From Virion Architecture to Pathogenesis. IJMS 2025;26:8323. https://doi.org/10.3390/ijms26178323.
[17] Landers VD, Thomas M, Isom CM, Karki D, Sokoloski KJ. Capsid protein mediated evasion of IRAK1-dependent signalling is essential to Sindbis virus neuroinvasion and virulence in mice. Emerging Microbes & Infections 2024;13:2300452. https://doi.org/10.1080/22221751.2023.2300452.
[18] Hatim C, Jebbari S, Benabbou A, Khibech O, Bezbaruah B, Ahmed B, et al. Synthesis, crystal structure and multi-scale computational investigation of 2-benzothiazolyl sulfide as a potential anti-HIV scaffold targeting gp120 and capsid proteins. Journal of Molecular Structure 2026;1374:146770. https://doi.org/10.1016/j.molstruc.2026.146770.
[19] Jebbari S, Omari M, Fouad MR, Mohammad-Salim H, Alaqarbeh M, Ben Ahmed A, et al. Synthesis and multiscale computational analysis of 6-nitrobenzoxazole-2-thione: electronic structure, intermolecular interactions, and predicted protease inhibition. New J Chem 2026;50:8856–67. https://doi.org/10.1039/D6NJ00979D.
[20] Benabbou A, Khibech O, Draoui Y, Bouhrim M, Ziyat H, Al-zharani M, et al. Multiscale in-silico profiling of phenoxy-acetamide: integrated ADME–Tox assessment, multi-target docking, molecular-dynamics validation, and Hirshfeld crystal analysis for antibacterial lead

optimization. Journal of Molecular Graphics and Modelling 2026;144:109330. https://doi.org/10.1016/j.jmgm.2026.109330.
[21] Pandey RK, Ojha R, Aathmanathan VS, Krishnan M, Prajapati VK. Immunoinformatics approaches to design a novel multi-epitope subunit vaccine against HIV infection. Vaccine 2018;36:2262–72. https://doi.org/10.1016/j.vaccine.2018.03.042.
[22] Ma S, Zhu F, Wen H, Rao M, Zhang P, Peng W, et al. Development of a novel multi-epitope vaccine based on capsid and envelope protein against Chikungunya virus. Journal of Biomolecular Structure and Dynamics 2024;42:7024–36. https://doi.org/10.1080/07391102.2023.2240059.
[23] Rahaman MdM, Hasan M, Jewel GMNA, Hasan S, Prodhan SH, Hoque H. Comprehensive immunoinformatics guided design and in silico assessment of a multi-epitope vaccine to elicit immunity against Mayaro virus. In Silico Pharmacol 2025;13:98. https://doi.org/10.1007/s40203-025-00387-5.
[24] Khatrawi EM, Ali SL, Althagafi H, Alqahtani HA. Antigenic Multi-Epitope Vaccine Against Ross River Virus Using Capsid and Envelope Proteins via Immunoinformatics and Reverse Vaccinology Approaches. Microbiology and Immunology 2026:1348-0421.70070. https://doi.org/10.1111/1348-0421.70070.
[25] Yan Z, Kim K, Kim H, Ha B, Gambiez A, Bennett J, et al. Next-generation IEDB tools: a platform for epitope prediction and analysis. Nucleic Acids Research 2024;52:W526–32. https://doi.org/10.1093/nar/gkae407.
[26] Greenbaum J, Sidney J, Chung J, Brander C, Peters B, Sette A. Functional classification of class II human leukocyte antigen (HLA) molecules reveals seven different supertypes and a surprising degree of repertoire sharing across supertypes. Immunogenetics 2011;63:325–35. https://doi.org/10.1007/s00251-011-0513-0.
[27] Kumar N, Tripathi S, Sharma N, Patiyal S, Devi NL, Raghava GPS. A method for predicting linear and conformational B-cell epitopes in an antigen from its primary sequence. Computers in Biology and Medicine 2024;170:108083. https://doi.org/10.1016/j.compbiomed.2024.108083.
[28] Doytchinova IA, Flower DR. VaxiJen: a server for prediction of protective antigens, tumour antigens and subunit vaccines. BMC Bioinformatics 2007;8:4. https://doi.org/10.1186/1471-2105-8-4.
[29] Dimitrov I, Bangov I, Flower DR, Doytchinova I. AllerTOP v.2—a server for in silico prediction of allergens. J Mol Model 2014;20:2278. https://doi.org/10.1007/s00894-014-2278-5.
[30] Martinelli DD. In silico vaccine design: A tutorial in immunoinformatics. Healthcare Analytics 2022;2:100044. https://doi.org/10.1016/j.health.2022.100044.
[31] Khatoon N, Pandey RK, Prajapati VK. Exploring Leishmania secretory proteins to design B and T cell multi-epitope subunit vaccine using immunoinformatics approach. Sci Rep 2017;7:8285. https://doi.org/10.1038/s41598-017-08842-w.
[32] Kandathil SM, Greener JG, Lau AM, Jones DT. Ultrafast end-to-end protein structure prediction enables high-throughput exploration of uncharacterized proteins. Proc Natl Acad Sci USA 2022;119:e2113348119. https://doi.org/10.1073/pnas.2113348119.
[33] Zhou X, Zheng W, Li Y, Pearce R, Zhang C, Bell EW, et al. I-TASSER-MTD: a deep-learning-based platform for multi-domain protein structure and function prediction. Nat Protoc 2022;17:2326–53. https://doi.org/10.1038/s41596-022-00728-0.

[34] Zheng W, Wuyun Q, Li Y, Liu Q, Zhou X, Peng C, et al. Deep-learning-based single-domain and multidomain protein structure prediction with D-I-TASSER. Nat Biotechnol 2026;44:641–53. https://doi.org/10.1038/s41587-025-02654-4.
[35] Ko J, Park H, Heo L, Seok C. GalaxyWEB server for protein structure prediction and refinement. Nucleic Acids Research 2012;40:W294–7. https://doi.org/10.1093/nar/gks493.
[36] Ponomarenko J, Bui H-H, Li W, Fusseder N, Bourne PE, Sette A, et al. ElliPro: a new structure-based tool for the prediction of antibody epitopes. BMC Bioinformatics 2008;9:514. https://doi.org/10.1186/1471-2105-9-514.
[37] Craig DB, Dombkowski AA. Disulfide by Design 2.0: a web-based tool for disulfide engineering in proteins. BMC Bioinformatics 2013;14:346. https://doi.org/10.1186/1471-2105-14-346.
[38] Bazhan SI, Antonets DV, Karpenko LI, Oreshkova SF, Kaplina ON, Starostina EV, et al. In silico Designed Ebola Virus T-Cell Multi-Epitope DNA Vaccine Constructions Are Immunogenic in Mice. Vaccines 2019;7:34. https://doi.org/10.3390/vaccines7020034.
[39] Shen Y, Maupetit J, Derreumaux P, Tufféry P. Improved PEP-FOLD Approach for Peptide and Miniprotein Structure Prediction. J Chem Theory Comput 2014;10:4745–58. https://doi.org/10.1021/ct500592m.
[40] Vangone A, Spinelli R, Scarano V, Cavallo L, Oliva R. COCOMAPS: a web application to analyze and visualize contacts at the interface of biomolecular complexes. Bioinformatics 2011;27:2915–6. https://doi.org/10.1093/bioinformatics/btr484.
[41] Chawla M, Kalra U, Petta A, Sharma S, Shaikh AR, Cavallo L, et al. *COCOMAPS* 2.0: a web server for identifying, analyzing, and visualizing atomic interactions at the interface of biomolecular complexes. Bioinformatics 2025;41:btaf606. https://doi.org/10.1093/bioinformatics/btaf606.
[42] López-Blanco JR, Aliaga JI, Quintana-Ortí ES, Chacón P. iMODS: internal coordinates normal mode analysis server. Nucleic Acids Research 2014;42:W271–6. https://doi.org/10.1093/nar/gku339.
[43] Kadukova M, Machado KDS, Chacón P, Grudinin S. KORP-PL: a coarse-grained knowledge-based scoring function for protein–ligand interactions. Bioinformatics 2021;37:943–50. https://doi.org/10.1093/bioinformatics/btaa748.
[44] Rapin N, Lund O, Castiglione F. Immune system simulation online. Bioinformatics 2011;27:2013–4. https://doi.org/10.1093/bioinformatics/btr335.
[45] Grote A, Hiller K, Scheer M, Munch R, Nortemann B, Hempel DC, et al. JCat: a novel tool to adapt codon usage of a target gene to its potential expression host. Nucleic Acids Research 2005;33:W526–31. https://doi.org/10.1093/nar/gki376.
[46] Andreano E, McLellan JS, Rappuoli R. Reverse vaccinology 3.0. Nat Rev Microbiol 2026;24:305–7. https://doi.org/10.1038/s41579-026-01286-y.
[47] Pizza M, Scarlato V, Masignani V, Giuliani MM, Aricò B, Comanducci M, et al. Identification of Vaccine Candidates Against Serogroup B Meningococcus by Whole-Genome Sequencing. Science 2000;287:1816–20. https://doi.org/10.1126/science.287.5459.1816.
[48] Hasan M, Ghosh PP, Azim KF, Mukta S, Abir RA, Nahar J, et al. Reverse vaccinology approach to design a novel multi-epitope subunit vaccine against avian influenza A (H7N9) virus. Microbial Pathogenesis 2019;130:19–37. https://doi.org/10.1016/j.micpath.2019.02.023.

[49] Jaiswal R, Kushawaha PK. Designing of a novel and potential multi-epitope-based vaccine using NS5 protein of dengue virus targeting all serotypes from India: An immunoinformatic approach. The Microbe 2025;7:100387. https://doi.org/10.1016/j.microb.2025.100387.
[50] Singha AK. Rational Design of a Multi-Epitope Ebola Vaccine Candidate Through Integrated Immunoinformatics and Structure-Based Analysis 2026. https://doi.org/10.21203/rs.3.rs-9834795/v1.
[51] Dunbar CA, Rayaprolu V, Wang JC-Y, Brown CJ, Leishman E, Jones-Burrage S, et al. Dissecting the Components of Sindbis Virus from Arthropod and Vertebrate Hosts: Implications for Infectivity Differences. ACS Infect Dis 2019;5:892–902. https://doi.org/10.1021/acsinfecdis.8b00356.
[52] Roy A, Swetha RG, Basu S, Biswas R, Ramaiah S, Anbarasu A. Integrating pan-genome and reverse vaccinology to design multi-epitope vaccine against Herpes simplex virus type-1. 3 Biotech 2024;14:176. https://doi.org/10.1007/s13205-024-04022-6.
[53] Biswas R, Swetha RG, Basu S, Roy A, Ramaiah S, Anbarasu A. Designing multi-epitope vaccine against human cytomegalovirus integrating pan-genome and reverse vaccinology pipelines. Biologicals 2024;87:101782. https://doi.org/10.1016/j.biologicals.2024.101782.
[54] Baseer S, Ahmad S, Ranaghan KE, Azam SS. Towards a peptide-based vaccine against Shigella sonnei : A subtractive reverse vaccinology based approach. Biologicals 2017;50:87–99. https://doi.org/10.1016/j.biologicals.2017.08.004.
[55] Samantaray M, Pushan SS, Rajagopalan M, Abrol K, Basumatari J, Murthy TPK, et al. Designing a multi-epitope vaccine candidate against pandemic influenza a virus: an immunoinformatics and structural vaccinology approach. Mol Divers 2025. https://doi.org/10.1007/s11030-025-11124-7.
[56] Alnajran H, Awadalla M, Aldakheel FM, Alam I, Momin AA, Alturaiki W, et al. Design of a peptide-based vaccine against human respiratory syncytial virus using a reverse vaccinology approach: evaluation of immunogenicity, antigenicity, allergenicity, and toxicity. Front Immunol 2025;16:1546254. https://doi.org/10.3389/fimmu.2025.1546254.
[57] Li J, Wang H, Wang L, Yu D, Zhang X. Stabilization effects of saccharides in protein formulations: A review of sucrose, trehalose, cyclodextrins and dextrans. European Journal of Pharmaceutical Sciences 2024;192:106625. https://doi.org/10.1016/j.ejps.2023.106625.
[58] Lopes Chaves L, Dourado D, Prunache I-B, Manuelle Marques Da Silva P, Tacyana Dos Santos Lucena G, Cardoso De Souza Z, et al. Nanocarriers of antigen proteins for vaccine delivery. International Journal of Pharmaceutics 2024;659:124162. https://doi.org/10.1016/j.ijpharm.2024.124162.
[59] Lu L, Yang M, Deng D, Shi X, Lovell JF, Jin H. Nanovaccines: Antigen selection, stabilization, adjuvantation, formulation, and evaluation. Coordination Chemistry Reviews 2025;541:216806. https://doi.org/10.1016/j.ccr.2025.216806.
[60] Freppel W, Koo YQ, Herrero LJ. A storm is born: immune activation and pathogenesis in arthritogenic alphavirus infections. Current Opinion in Virology 2026;74:101498. https://doi.org/10.1016/j.coviro.2025.101498.